Deep–Sea Research I 232 (2026) 104758

Contents lists available at ScienceDirect

Deep-Sea Research Part I

journal homepage: www.elsevier.com/locate/dsri

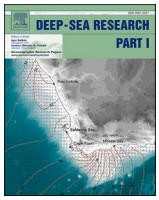

High-resolution species distribution modelling of the vulnerable marine ecosystem indicator species, *Enallopsammia rostrata*, on Walvis ridge, SE Atlantic

Lisa Skein [a,b,c,*], Sarah Paulus [d], Erich Maletzky [d], Paulus Kainge [d], Covadonga Orejas [e], F. Javier Murillo [f], Christian Mohn [g], Roberto Sarralde [h], Tabitha R.R. Pearman [a], Tobias Endjambi [d], Veerle A.I. Huvenne [a]

[a] *Marine Science, National Oceanography Centre, United Kingdom*
[b] *Nelson Mandela University, Centre for Coastal and Marine Research, South Africa*
[c] *South African National Biodiversity Institute, Marine Programme, South Africa*
[d] *National Marine Information and Research Centre (NatMIRC), Ministry of Agriculture, Fisheries, Water and Land Reform, Swakopmund, Namibia*
[e] *Centro Oceanográfico de Gijón, Instituto Español de Oceanografía (IEO-CSIC), Spain*
[f] *Fisheries and Oceans Canada, Bedford Institute of Oceanography, Dartmouth, NS, Canada*
[g] *Department of Ecoscience, Aarhus University, Roskilde, Denmark*
[h] *Centro Oceanográfico de Vigo, Instituto Español de Oceanografía (IEO-CSIC), Spain*

ARTICLE INFO

Keywords:
Areas beyond national jurisdiction
Cold-water corals
Enallopsammia rostrata
Kinetic energy dissipation
Species distribution modelling
Vulnerable marine ecosystems
Walvis ridge

ABSTRACT

Knowledge on the distribution of Vulnerable Marine Ecosystems (VMEs) is critical to support their effective management. However, major knowledge gaps still exist, particularly in Areas Beyond National Jurisdiction (ABNJ). Species Distribution Models (SDMs) can help to fill these gaps, especially in historically under-sampled regions. The Walvis Ridge in the South-East Atlantic, for example, consists of extensive seamount complexes and hosts deep-sea fauna that constitute VMEs, but is among the most data-poor globally.

Presence/background models predicting the occurrence of the cold-water coral *Enallopsammia rostrata*, the most frequently encountered VME indicator species in the area to date, were developed for Valdivia Bank and Ewing seamount (NE Walvis Ridge). We found that incorporating high-resolution hydrodynamic variables and applying modifications to compensate for class imbalance in presence/background models strengthened models and reduced uncertainty. Random Forest models generally outperformed MaxEnt models, but an ensemble model had the best overall performance. The ensemble model predicted that 4.45% (10 519.90 km^2) of the study area has suitable habitat for *E. rostrata*, driven by depth, slope, kinetic energy dissipation and downwelling intensity.

We demonstrate that even when developed on smaller occurrence record datasets, SDMs can deliver useful predictions, given appropriate statistical compensations and the addition of high-resolution hydrodynamic variables. The maps produced represent a valuable addition to ongoing spatial planning in this ABNJ, and can guide future survey effort aiming to validate, strengthen and broaden SDMs to improve our understanding of the distribution of VMEs in the under-studied SE Atlantic.

1. Introduction

Sustainable management of ecologically important deep-sea habitats in Areas Beyond National Jurisdiction (ABNJ) is of increasing global importance, but the biodiversity in these habitats is among the most poorly studied (Bell et al., 2025; Glover et al., 2018). The recently ratified Biodiversity Beyond National Jurisdiction (BBNJ) Agreement emphasises the use of Area-Based Management Tools (ABMTs), such as Marine Protected Areas (MPAs), as important conservation measures to sustainably manage seabed use in the high seas (United Nations, 2023). However, large knowledge gaps on the spatial distribution of deep-sea biodiversity substantially limits the ability to implement meaningful ABMTs.

Among the existing mechanisms that aim to safeguard important

* Corresponding author. Marine Science, National Oceanography Centre, United Kingdom.
E-mail address: lisa.skein@noc.ac.uk (L. Skein).

https://doi.org/10.1016/j.dsr.2026.104758
Received 20 February 2026; Received in revised form 16 September 2026; Accepted 17 September 2026
Available online 18 September 2026

deep-sea habitats are those outlined by the Food and Agriculture Organization (FAO) for fisheries that operate in ABNJ, most of which are managed by relevant Regional Fisheries Management Organisations or Arrangements (RFMO/As). The FAO guidance came in response to Resolution 61/105 of the United Nations General Assembly (UNGA, 2006), where member states and RFMO/As are called upon to protect and prevent any significant adverse impacts to Vulnerable Marine Ecosystems (VMEs); ecosystems that are highly vulnerable to destructive seabed activities such as bottom fishing. The FAO guidance lists several criteria to designate VMEs, along with a non-exhaustive list of example species, communities and habitat features that can support VMEs (FAO, 2009).

Framework-forming cold-water corals (CWC) and the summits and flanks of seamounts, guyots, banks, knolls and hills are among indicative VME taxa and habitat types, respectively, described in the FAO guidelines as in need of protection from bottom fishing practices (FAO, 2009). Highly heterogenous terrain in combination with dynamic water movement at such areas can create ideal environments for suspension-feeding fauna like CWC (Morato et al., 2021; Mortensen et al., 2008; Tracey et al., 2011). CWC frameworks are highly fragile, which in combination with slow growth rates (Lartaud et al., 2017), extreme longevity (Etnoyer et al., 2018; Hitt et al., 2020), and slow or limited recruitment (Strömberg and Larsson, 2025) render them highly vulnerable to destructive activities like bottom trawling (Hinz, 2017). Studies investigating CWC habitats degraded by bottom trawling estimate that recovery can take anything from decades to centuries (Baco et al., 2019; Bett et al., 2025; Clark et al., 2016, 2019), if at all. Biogenic frameworks formed by CWCs increase physical habitat complexity (Cordes et al., 2008) and create environmental niches for many other taxa that utilise them for attachment, feeding, shelter, reproduction and predator avoidance (Buhl-Mortensen et al., 2010; Costello et al., 2005; Rogers et al., 2007; Stevenson et al., 2015). This enhances biomass and diversity (Demopoulos et al., 2014; Van Oevelen et al., 2009), and many taxa have been shown to be either fully dependent on or strongly associated with deep-sea CWCs (Corbera et al., 2019; Henry and Roberts, 2007; Jonsson et al., 2004; Price et al., 2019). This also applies to species of commercial interest. In a recent review, Selgrath et al. (2026) revealed that approximately 30% of the commercially landed species in California were associated with framework-forming CWC, emphasizing their role as essential fish habitats. For these reasons the destruction of CWC habitats translates into significant decreases in the diversity, richness and abundance of associated benthic communities (Althaus et al., 2009; Koslow et al., 2001), alongside the loss of the vital ecosystem services they provide (La Bianca et al., 2023).

To date, limited knowledge on the distribution of VMEs in ABNJ has

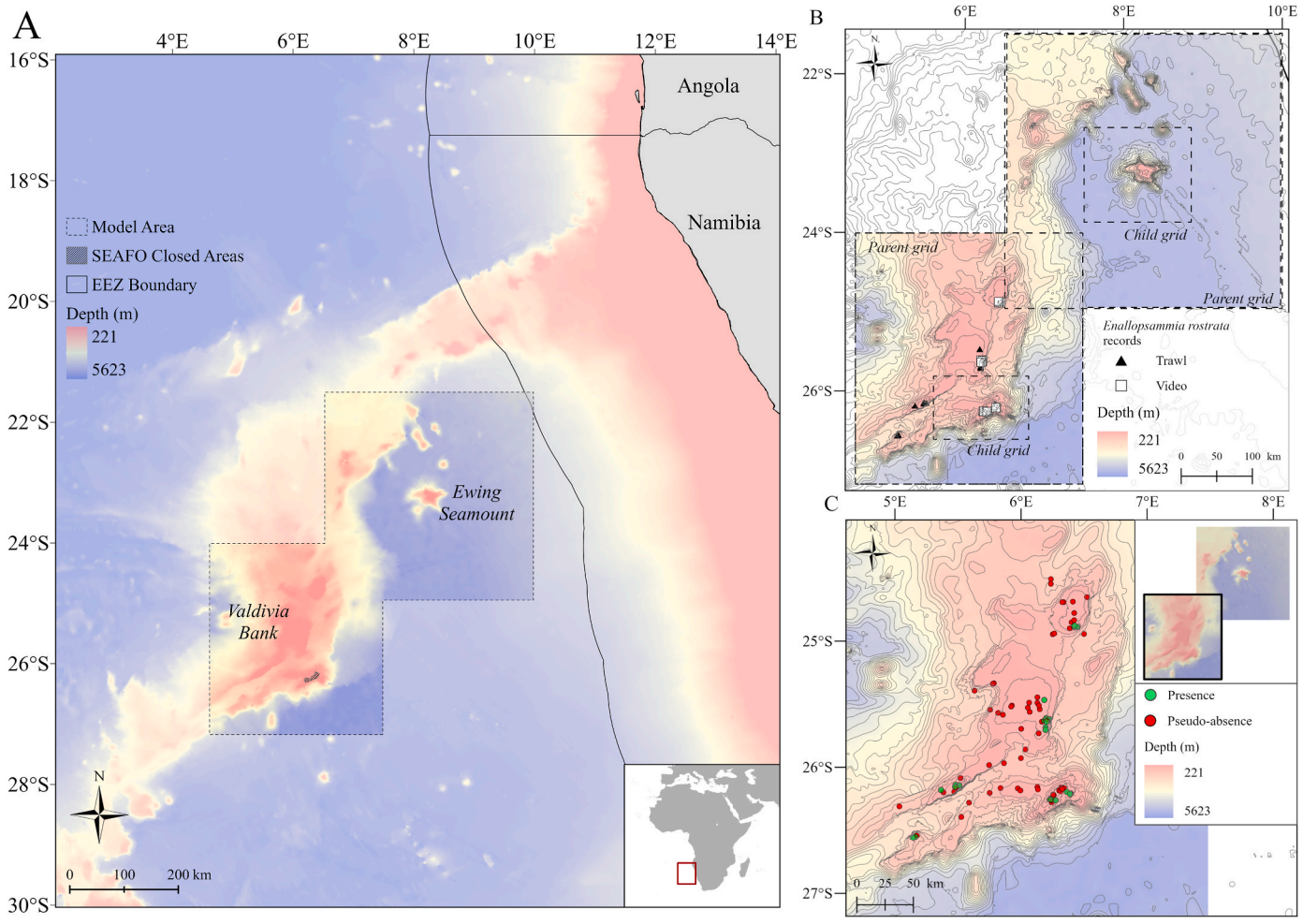

Fig. 1. (A) The north-eastern portion of the Walvis Ridge with ABNJ focus areas for this study (Valdivia Bank and Ewing seamount), as well as SEAFO bottom fishing and SEAFO closed areas. Note this does not show the entire SEAFO-CA and all fished/closed areas. Underlying bathymetry is GEBCO (GEBCO Bathymetric Compilation Group, 2020).(B) Predictive models were trained on occurrence records of *Enallopsammia rostrata* on Valdivia Bank, and transferred onto Ewing Seamount, generating predictions across both areas. Hydrodynamic variables were extracted at 500m resolution at topographically complex areas (Child grids), and at 1500 m resolution across broader areas (Parent grids). (C) Model development extent on Valdivia Bank showing *Enallopsammia rostrata* presence and pseudo-absence points.

made implementation of the required protection measures challenging (Du Preez et al., 2020). Whilst ABNJ are generally data-poor, this is even more pronounced at regions like the South-East Atlantic (Menegotto and Rangel, 2018; Bridges et al. 2023a, 2023b). In this region, a feature of particular interest and relevance to VMEs is the Walvis Ridge that extends from the Namibian shelf south-westward towards the Mid-Atlantic Ridge, the majority of which falls within ABNJ (Fig. 1). This system consists of seamounts, guyots, canyons and embayments (Contreras et al., 2022) and represents a barrier between North Atlantic Deep Water and Antarctic Bottom Water (Pérez-Díaz and Eagles, 2017). The Walvis Ridge is recognised as an Ecologically and Biologically Significant Area (EBSA) by the Convention on Biological Diversity (Secretariat of the Convention on Biological Diversity, 2020), meaning it is regarded as critically important for the functioning of marine ecosystems.

With its complex morphology and high productivity, the Walvis Ridge is home to diverse suspension- and filter-feeding benthic communities that likely constitute VMEs (Baco et al., 2023). The first reports of VME indicator taxa from this area, specifically scleractinian CWCs, originated from research cruises that took place in 1982 – 1984, although the survey methodology at the time has since been described as inadequate for the sampling of these taxa (Zibrowius and Gili, 1990). More recent efforts focused on benthic communities include Spanish-Namibian expeditions from 2008 to 2010 (López Abellán and Holtzhausen, 2011; Muñoz et al., 2012) and one other led by the Ecosystem Approach to Fisheries (EAF)-Nansen Programme in 2015 (FAO, 2016). In light of the findings from these latter efforts, the South-East Atlantic Fisheries Organisation (SEAFO), the relevant RFMO/A in this area, applied a precautionary approach by implementing bottom fishing closures for 11 areas and a partial closure in one area that still allows pots and bottom longlines (located on the southern edge of Valdivia Bank) where VMEs may be present, as detailed in SEAFO Conservation Measure (CM) 30/15 (www.seafo.org). In the absence of more detailed information, the closures implemented through CM 30/15 were underpinned by coarsely identified geomorphological features that may support VMEs. At the same time, all fishing activity in the SEAFO Convention Area remains concentrated on seamounts (Fig. 1). Most of the current closures are at depths below 1000 m, although the partial closure at Valdivia Bank South, which falls inside the area focused on in this study, spans a depth range of 414 – 996 m according to the latest high-resolution bathymetry for this area.

Only three published studies thus far describe some aspects of benthic communities on Walvis Ridge (Bergstad et al., 2019a; Gil and Ramil, 2021; Zibrowius and Gili, 1990), the most comprehensive of which, at the time of this publication, is that by Bergstad et al. (2019a). It described the observed dominance of scleractinian CWCs, particularly of *Enallopsammia rostrata* (Pourtalès, 1878) (Fig. 2), followed by Gorgonian and Antipatharian corals, as well as commercially important fish and invertebrates. *E. rostrata*, as part of the family Dendrophylliidae, can create large dendroid colonies up to 1 m wide and ~0.5 m tall and is regarded as one of the most significant habitat-forming CWC taxa globally (Freiwald et al., 2004). Like other deep-sea scleractinian corals, *E. rostrata* exhibits extreme longevity, with some live specimens estimated to be over 100 years old in one study (Adkins et al., 2004), and between 209 and 605 years old in another study (Houlbrèque et al., 2010). Its growth rates have been estimated at 0.012 – 0.072 mm/y which is slower than that of other frequently studied scleractinian species like *Desmophyllum pertusum* or *Madrepora oculata* (Houlbrèque et al., 2010; Montero-Serrano et al., 2013).

Species Distribution Modelling (SDM), or habitat suitability modelling, is a key tool that is being used to generate predictions of spatial distribution patterns of VME indicator taxa in understudied deep-sea regions (Ardron et al., 2014). Predictive SDM maps covering large portions of un-surveyed areas are especially useful in supporting spatial management planning (Georgian et al., 2019; Rowden et al., 2017) and to guide targeted field surveys in under-explored areas (Georgian et al., 2014). To date, no local-scale models have been developed at high resolution for VME indicator taxa, like *E. rostrata*, for the Walvis Ridge. Existing SDMs for *E. rostrata* developed elsewhere suggest that the

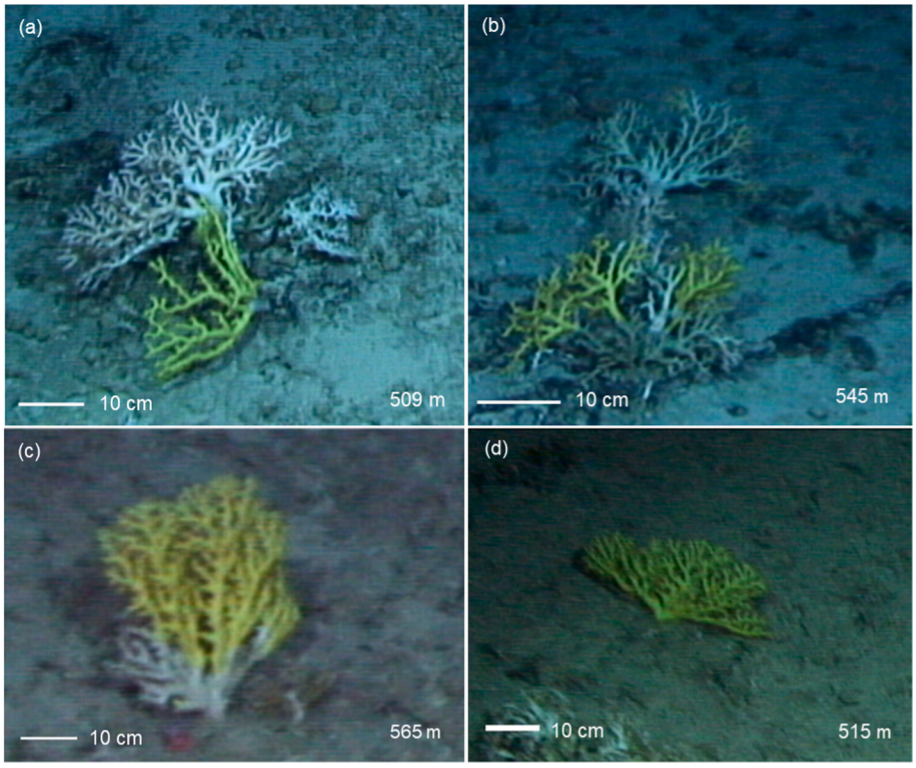

Fig. 2. Examples of *Enallopsammia rostrata* records identified from video transects performed in 2015 (FAO, 2016). Images from Dive 13 (A, B), Dive 10 (C), and Dive 16 (D) on Valdivia Bank.

distribution of this species tends to be patchy and concentrated to the steep slopes of ridge-like features and seamount chains (Georgian et al., 2019; Rowden et al., 2017; Tracey et al., 2011; Vinha et al., 2024). Water column properties such as bottom salinity have also been suggested to be an important environmental driver of its distribution (Anderson et al., 2016; Tong et al., 2023; Vinha et al., 2024), potentially linked to the influence of distinct water masses on CWC distribution (Puerta et al., 2020). For example, modelling outputs produced in Vinha et al. (2024) suggested that depths with elevated salinity values that *E. rostrata* appeared to favour corresponded to the distribution of North Atlantic Deep Water in Cabo Verde, between 1200 and 1700 m. Ideal depth ranges for this species in the South Pacific, on the other hand, are predicted to be between 500 and 1500 m (New Zealand; Tracey et al., 2011). Global-scale models for *E. rostrata* suggest a broad depth distribution, from surface waters to beyond 1000 m (Davies and Guinotte, 2011; Tong et al., 2023), although on Walvis Ridge Bergstad et al. (2019a) suggest that it likely inhabits a narrower range, between 350 and 800 m.

In the absence of local-scale or sub-regional scale SDMs, global-scale models are useful and especially so in areas with no existing survey data. However, global-scale models tend to be developed at comparatively coarser resolutions and often with environmental variables lacking local validation. Mismatches between the resolutions at which global models are developed and resolutions relevant for management, combined with an overprediction tendency (Tong et al., 2023) and a lack of local data to underpin model development, can all together result in limited stakeholder uptake and limited effectiveness of such maps in supporting local spatial plans (Winship et al., 2020). Coarse resolution environmental variables limit the ability of such models to capture the fine-scale environmental heterogeneity that can influence the occurrence of VME indicator taxa like CWCs (Lecours et al., 2015; Rengstorf et al., 2013; Yánez-Suárez et al., 2024).

Environmental variables that describe the transport and delivery of organic matter to CWC, as food, are important in models developed for suspension-feeding taxa (Mohn et al., 2014; Pearman et al., 2020). Hydrodynamic variables that describe these processes can strengthen model performance and improve prediction accuracy (Pearman et al., 2020; Rengstorf et al., 2014). However, these variables are seldom available at high resolution, and so other proxies derived from bathymetry are often used. In a study where an original model for the sponge *Pheronema carpenteri* was validated using newly collected data, the authors suggested that among the likely reasons for the poor performance of the model was indeed the omission of hydrodynamic variables related to food supply (Howell et al., 2022). Mohn et al. (2025) recently developed a high-resolution hydrodynamic model for the NE portion of the Walvis Ridge (specifically covering Valdivia Bank and Ewing seamount) that describes near-bottom currents and physical processes. By integrating the available high-resolution bathymetry across the more topographically complex sections of Valdivia Bank and Ewing Seamount, the study refined variations in near-bottom currents at these areas. The study also explored potential causal links between some of the modelled hydrodynamic properties and the distribution of CWC and sponge taxa that were recorded during the 2008 – 2010 RAP-SUR expeditions (López Abellán and Holtzhausen, 2011). Areas with intensified kinetic energy dissipation and internal wave dynamics corresponded with greater occurrences of CWCs and sponges (Mohn et al., 2025), highlighting the potential value of such variables in predictive SDMs for these taxa.

With this set of valuable environmental variables, it is now possible to develop the first high-resolution predictive model for a deep-sea VME indicator species, i.e. *E. rostrata*, for this portion of the Walvis Ridge. Although *E. rostrata* is currently the VME indicator species with most occurrence records in the area (and the only such species that currently has a sufficient number of local records to enable model development), the limited historical survey effort in the area means that the number of records is still relatively low. However, as the field of SDM and specifically its application to data-limited regions has progressed, so too has the ability to statistically compensate for algorithm-specific limitations associated with smaller datasets. Deep sea SDMs rarely have accurate information on true absences, so presence/pseudo-absence or presence/background modelling approaches like Maximum Entropy (MaxEnt) (Elith et al., 2011; Phillips et al., 2006) are often used (Ashford et al., 2014; Shantharam et al., 2025; Wiltshire et al., 2018). However, MaxEnt can tend to overpredict and handles correlated variables comparatively worse than tree-based classification approaches (Zhao et al., 2022) such as Random Forest (RF) (Breiman, 2001). Whilst there are other advantages to using RF, it is not explicitly designed for presence/background modelling, and it can have poor performance when presences are substantially outnumbered by background or pseudo-absence points (Barbet-Massin et al., 2012; Liu et al., 2019; Valavi et al., 2022), such as in a scenario with few presence records. Modifications in which the RF algorithm uses environmental information at presence and background locations have been put forward by Valavi et al. (2021), and were used in this study. Finally, in cases where the choice between individual algorithms may not be clear, and/or to mitigate variability the predictions delivered by different algorithms, ensemble models can be used (Robert et al., 2016).

The aims of this study were therefore to (i) develop the first high-resolution SDM for the VME indicator species, *E. rostrata* on Walvis Ridge, (ii) compare performance of presence/background algorithms and the effect of integrating high-resolution hydrodynamic variables, (iii) explore effects of resampling modifications on the performance of RF models when developed in a presence/background mode, and (iv) investigate the relationship of environmental variables and *E. rostrata* occurrence on Walvis Ridge.

2. Methods

2.1. Study area

The Walvis Ridge system in the South-East Atlantic is an aseismic volcanic chain with diverse geomorphological features including banks, seamounts, guyots and canyons. The north-eastern origin of the ridge is on the Namibian continental margin from where it extends into the ABNJ in a south-western direction to near the Mid-Atlantic Ridge at the Tristan da Cunha and Gough islands. This study focused on the north-eastern ABNJ portion of Walvis Ridge, specifically Valdivia Bank and Ewing seamount (Fig. 1). Valdivia Bank is a large plateau with a depth range of 220 m to > 4000 m into the surrounding abyssal plains (Bergstad et al., 2019b; Contreras et al., 2022). The majority of Valdivia Bank has gentle slopes (<1°), but this increases at several mounds with steep sides (>15°), as calculated from the latest high-resolution (150 m) merged bathymetry grid of this area (Contreras et al., 2022). These mounds vary between 220 and 440 m in height, with mound summits at depths between 500 and 1330 m. Steeper slopes (10 – 30°) are observed at small knolls that cap some of these mounds (Contreras et al., 2022). To the northeast of Valdivia Bank lies Ewing Seamount (23°14.7′S, 08°16.0′E); an irregularly shaped, isolated seamount with a summit depth of 780 m and a summit plateau with depths between 850 and 1000 m (Fig. 1). From its south-eastern summit in a north-west direction runs a wide, elongated plateau that drops off drastically in the north-west at about 950 m (Bergstad et al., 2019b).

2.2. Data collection

2.2.1. Environmental variables

Shipboard multibeam echosounder (MBES) data collected during the 2008 – 2010 RAP-SUR and 2015 EAF-Nansen expeditions covered the more topographically complex areas in the study area and importantly the confirmed presence locations of *E. rostrata*. Acoustic data were cleaned via Caris (Hips & Sips) software and a merged bathymetry grid was produced at an initial 50 m resolution, with data gaps filled by the

mean value of neighbouring pixels. This grid was subsequently merged with the GEBCO_2020 global bathymetry layer (GEBCO, 2020) to create a uniform bathymetry layer at a 250 m resolution. The GEBCO_2020 grid represents a non-blended compilation of bathymetry from GEBCO's global terrain model and sparse bathymetry datasets supplied by international and national data repositories. From the merged MBES bathymetry and GEBCO_2020 grid, bathymetry-derived terrain variables were calculated using the 'terra' R package (Hijmans et al., 2026).

Information on the nature of the terrain such as seabed roughness, as well as the relative positioning of a grid cell in relation to neighbouring cells, also provide useful information on the likely suitability of an area to support the attachment of a particular species (Dolan et al., 2008; Wilson et al., 2007). This included slope (maximum change in elevation over the distance between a cell and its neighbouring cells), aspect (i.e. orientation of the slope, converted into eastness (sin*(aspect)*) and northness (cos*(aspect)*), Terrain Ruggedness Index (TRI; local variation in the terrain around a central pixel, an estimate of terrain heterogeneity), Topographic Position Index (TPI; elevation of a cell in relation to the average elevation of neighbouring cells) and curvature (profile curvature, i.e. curvature of the surface in the steepest down-slope direction) (Table 1). Slope, TPI and TRI were calculated using a 3 x 3 cell window (Wilson et al., 2007).

Hydrodynamic variables (3-D velocities, 3-D density field) were extracted from simulations of the ROMS-AGRIF model (version 3.1) for Valdivia Bank and Ewing seamount. Variables were derived at higher resolution in more topographically complex areas (child grids, 500 m resolution), nested within the wider area where variables were derived at coarser resolution (parent grids, 1500 m resolution) (Fig. 1b). The use of the 500 m resolution child grids at geomorphologically complex areas with existing fine resolution bathymetry resolves greater small-scale variability and localised flow features at these areas, whereas the 1500 m resolution parent grids capture dominant spatial patterns, large-scale gradients, and the main kinetic energy dissipation hotspots (Mohn et al., 2025). All parent and child grids employ 32 terrain-following vertical layers, with increased resolution near the surface and close to the seafloor. Near-bottom vertical resolution ranges from < 2 to 39.5 m at Valdivia Bank and from 6.5 to 38 m at Ewing seamount. The highest vertical resolution can be found in shallower, topographically more complex areas. More detail on the development and local validation of this model can be found in Mohn et al. (2025). Inverse Distance Weighting (IDW) with a 16 - cell search radius was used to interpolate and subsequently merge parent and child grids to a 250 m resolution, matching that of the bathymetry grid. Bottom temperature, bottom salinity, horizontal current speed of the bottommost layer, kinetic energy dissipation of the bottommost layer (as a proxy for vertical mixing and encounter rates of particles, indicative of food availability), internal wave slope criticality (internal wave propagation direction and intensity, related to mixing and distribution of food particles), and vertical velocity (indicative of upwelling/downwelling intensity) were extracted as daily averages for the year 2009. All environmental layers used in modelling were in continuous raster format in a WGS 1984 datum and with a cell size of 0.00225° equating to approximately 250 m resolution (Fig. S1).

Table 1
Terrain-, oceanographic- and hydrodynamic variables considered for models. *Variables retained in final models. ** Profile curvature was used in terrain variable-only models but was excluded from models combining terrain- and hydrodynamic variables. Terrain variable only models used all terrain variables apart from TRI.

Environmental variable	Resolution	Unit
Terrain		
Depth *	250 m	Meters
Slope *		Degrees
Eastness *		
Northness *		
Profile curvature **		
Topographic Position Index (TPI) *		
Terrain Ruggedness Index (TRI)		
Hydrodynamic		
Maximum Bottom Temperature (2009)	Higher resolution (500 m) small model domain (child grid) embedded in lower resolution larger model domain (parent grid). Interpolated through Inverse Distance Weighting to 250 m.	°C
Mean Bottom Temperature (2009)		°C
Minimum Bottom Temperature		°C
Maximum Bottom Salinity (2009)		PSU
Mean Bottom Salinity (2009)		PSU
Minimum Bottom Salinity (2009) *		PSU
Maximum Horizontal Current Speed (2009)		m/s
Mean Horizontal Current Speed (2009)		m/s
Minimum Horizontal Current Speed (2009)		m/s
Mean Kinetic Energy Dissipation – Bottom (2009) *		$\log_{10}$ ε (W/kg)
Maximum Annual Vertical Velocity (2009)		m/s
Mean Annual Vertical Velocity (2009)		m/s
Minimum Annual Vertical Velocity (2009) *		m/s
Mean Internal Wave Slope Criticality (2009)		m/s

2.2.2. *Enallopsammia rostrata* distribution

Information on the geographic distribution of *Enallopsammia rostrata* was gathered through various sources. Spanish-Namibian research cruises between 2008 and 2010 under the RAP-SUR project took place aboard the B/O Vizconde de Eza and collected physical samples through bottom rock dredge trawls (López Abellán and Holtzhausen, 2011), among which *E. rostrata* was described as a frequently observed and dominant species. In total, 14 geo-referenced records were assigned to *E. rostrata*, representing the coral species with the most occurrence records from the area at the time. One more record was retrieved from the OBIS database, originating from the first study that mentioned scleractinian corals on Walvis Ridge (Zibrowius and Gili, 1990).

A 2015 expedition carried out under the EAF-Nansen Programme of the FAO aboard the R/V Dr Fridtjof Nansen focused on data collection to describe VME habitats as well as commercially valuable species within the SEAFO-Convention Area (FAO, 2016). This expedition used a towed video rig to conduct visual survey transects across several seamounts in the SEAFO-CA. Of specific relevance to this study are transects on Valdivia Bank ($n = 20$) and Ewing seamount ($n = 5$) (Table A1, and more information can be found in FAO (2016) and Bergstad et al. (2019a)). Each transect followed an upslope direction at speeds between 0.5 and 1.5 kts, and replicate lines covered approximately 0.9 – 1.7 km (0.5 to 0.9 nm). For this study, the raw video footage from the transects was processed to establish potential *E. rostrata* records, which were subsequently confirmed by taxonomic experts (Fig. 2). Dive tracks from the survey were reconstructed using time-stamped positional information recorded by the camera system's software, and the observed occurrences of *E. rostrata* were time-matched with the dive times to provide occurrence coordinates. A total of 25 additional records were confirmed from the video transects (Table A1), 16 of which were added to the modelling dataset to ensure that one record per 250 m grid cell was used during model development. Results from opportunistic Van Veen grabs deployed during the 2015 survey delivered one additional record, although this also had to be discarded as an existing visual record was already present within the particular grid cell. A final 32 occurrence

records for *E. rostrata*, all located on Valdivia Bank, were used for model development (Fig. 1b and c).

2.3. Species distribution models

2.3.1. Variable selection

All analyses were performed in RStudio (Posit team, 2026). MaxEnt, RF, and ensemble models merging predictions from the best-performing iterations of each MaxEnt and RF model were used to generate predictions of *E. rostrata* occurrence for this section of Walvis Ridge. As all available presence records of *E. rostrata* were from Valdivia Bank, models were developed for this area and then transferred onto Ewing seamount, for which the same environmental variables were available to enable model transfer. Modelling extent was dictated by the extent at which hydrodynamic variables were produced (parent and child grids, Fig. 1b). The overlapping area between the Valdivia and Ewing parent grids was masked from the Ewing raster datasets and used for model development focused on the Valdivia Bank area (Fig. 1b and c). Selection of variables to be included in final models was done by removing strongly correlated variables (Pearson correlation coefficient > 0.7) and those with a variation inflation factor (VIF) > 5. A set of variables with VIF scores < 5 can be regarded as having a low level of co-linearity (Heiberger and Holland, 2004) and is often used to aid variable selection in SDM studies (Yesson et al., 2017). A preliminary MaxEnt model was first run on the full set of variables (Table 1), after which particular variables that were part of a strongly correlated pair and contributed the least to model AUC were systematically removed ('SDMTune' R package (Vignali et al., 2020)), and until the VIF scores for the remaining variables were < 5 (Zuur et al., 2009).

2.3.2. Extrapolation analysis

Areas characterised by environmental conditions outside of the observed model training data, i.e. areas of model extrapolation, were identified to provide additional insight on the degree to which model training data represents the environmental conditions of the prediction area. This is also useful to identify areas where the reliability of model predictions may be limited (i.e. extrapolated/non-analogous areas) and where future sampling efforts can be prioritised. This was done using the Extrapolation Detection (ExDet) tool (Mesgaran et al., 2014) from 'dsmextra' R package (Bouchet et al., 2020). Cells identified as having non-analogous conditions to those in the observational dataset can be so assigned as a result of univariate (outside the range of one variable) or combinatorial (novel combinations of between variables) extrapolation (Mesgaran et al., 2014). Cells with both univariate and combinatorial extrapolation are categorised as univariate, in which case the variable with the greatest univariate distance is recognised as the most influential variable for the cell. The relative percentage of extrapolated area attributed to variables responsible for univariate and combinatorial extrapolation was also summarised (Table S2). Further visual depiction of the ranges of environmental variables across the prediction area and those at observed points used for model development is included in the supplementary material (Fig. S3).

2.3.3. Role of environmental variables

To investigate the effects of incorporating high-resolution hydrodynamic variables on model outputs, separate MaxEnt and RF models were developed on terrain-only and combined terrain-hydrodynamic datasets. The performance of the respective models (terrain variable-only vs terrain-hydrodynamic variables) was compared by contrasting their predictions, their respective rankings of environmental variables, model evaluation metrics, and in terms of how realistic they captured likely species-environment relationships.

Functional response curves depicting the relationship between the predicted probability of *E. rostrata* occurrence and environmental variables used in modelling were constructed through extraction of predicted occurrence probability values across ranges of those environmental variables included in the model. Locally estimated scatterplot smoothing was subsequently applied to generate response curves with accompanying 95% confidence intervals.

Proportional importance of variables in each model was informed following the approach described in Thuiller et al. (2016), and recently applied, for example, in a similar study by Vinha et al. (2024). In this approach, (1) predictions are made with the original model training data, (2) the order of values of one variable is permuted whilst those of the remaining variables are kept as is, (3) a new prediction is made with the permuted variable, (4) the correlation between predictive values of the original prediction and the predicted values made with the permuted variable is assessed. In this case, low correlation scores indicate that the permuted variable has a strong effect on the model's prediction, and vice versa.

Variables with low importance will produce higher correlation scores, whereas those with greater importance will drive lower correlation scores. Modelling algorithms often have different measures of variable importance; however, this approach allows for a standardised evaluation of importance across algorithms, including those used in the present study.

2.3.4. Modelling algorithms

MaxEnt is a presence-only algorithm that uses presence and 'background' points to characterise environmental conditions across an area. The algorithm aims to minimise distance between probability densities where species/habitats are present and the environmental variables (Elith et al., 2011; Phillips and Dudík, 2008). To account for potential effects of sampling bias, background points ($n = 1000$) were generated via Kernel Density Estimation (KDE) with default bandwidth selection settings using the 'MASS' package (Venables and Ripley, 2002) which concentrates background points around presence points. MaxEnt models were subsequently developed with terrain variables only as well as a combination of terrain and hydrodynamic variables, using default parameters. This was done through the R packages 'rJava' (Urbanek, 2026), 'raster' (Hijmans, 2025), and 'dismo' (Hijmans et al., 2024) and the open-source MaxEnt software (Phillips et al., 2017).

The machine-learning RF algorithm generates decision-trees across covariate space, using ensembles from hundreds to thousands of trees to produce qualitative (classification) or quantitative (regression) predictions (Breiman, 2001). RF deals reasonably well with correlated variables, include interactions in the fitted model, and are flexible in the type of data that can be used (Elith, 2019). It can be developed on presence/absence or presence/pseudo-absence points; with "pseudo-absences" often used interchangeably with "background" points. The choice of background points for RF model development was informed by trawl locations where *E. rostrata* was not recorded during the 2008-2010 RAP-SUR expeditions ($n = 70$). It is recognised that these points do not represent true absences across a grid cell, however the use of these points was deemed sensible as it similarly aims to account for potential effects of sampling bias as done by KDE-generated background points used for the MaxEnt models.

In comparison to traditional presence/background models, RF can be sensitive to imbalanced classes, for example when the background or pseudo-absence points substantially outnumber the presence points (Johnson et al., 2012; Robinson et al., 2018; Valavi et al., 2022). In this study, we explored the effects of potential solutions to such problems in RF presence/background models as suggested in Valavi et al. (2021). This included (i) the application of weights to each class, where the cost of misclassifying the minority class (i.e. presences) is increased, here applied to the Gini index (ii) an equal-sampling approach, where different subsampled datasets are generated from the original, each with equal classes and thus subsampling the pseudo-absence points, and (iii) a down-sampling approach, where the same number of presence and pseudo-absence points are used but at the level of each individual tree, and sampled by replacement (i.e. bootstrapping) from the full dataset, therefore allowing the use of more pseudo-absence points. The

advantage of down-sampling as opposed to equal sampling is that because of the bootstrapping approach, many more of the pseudo-absence points can be used and so a better characterisation of background conditions can be informed while at the same time compensating for class imbalance. Before doing so, however, the effects of hydrodynamic variables on RF models were investigated by comparing outputs from RF models run in default mode, with and without hydrodynamic variables. After it was revealed that inclusion of hydrodynamic variables resulted in predictions much less influenced by bathymetry-related noise, with lower uncertainty, and with mostly minor differences in evaluation metrics, the decision was made to further explore the effect of resampling modifications described above on RF models that included hydrodynamic variables. The code used for resampling modifications is provided in Valavi et al. (2021).

Optimal model parameters were determined using the tuneRF function from the 'randomForest' package (Liaw and Wiener, 2002) on the 5 x 10 cross-validated training data (see below), whereby the influence of the number of variables used at each split (mtry) on out-of-box error rates was investigated. This value was then used to determine the number of trees (ntree) that would also result in the lowest error rates. Optimal parameters were thus mtry = 2, ntree = 500, and models were run in classification mode.

2.3.5. Model evaluation

Models were developed on a 5 x 10 cross-validation approach, where data is split into five folds ('dismo' package; Hijmans et al., 2024), trained on four of the five folds and tested on the remaining fold, with this process repeated 10 times, each time with different combinations of points assigned to folds. MaxEnt and ensemble models were tested on the same testing data than that used in RF models (presence/pseudo-absence points). Rasters of predicted probabilities produced through each modelling approach were averaged across the 5 x 10 cross-validated replicates, with accompanying uncertainty presented by the proportional coefficient of variation surrounding the mean.

Model performance was evaluated through threshold-independent and threshold-dependent metrics, visual inspection of the nature of the predictions produced, and prediction uncertainty. The threshold-independent metric was the Area Under the Curve (AUC) of the receiver operating curve, where AUC $>$ 0.7 is reflective of good discriminatory ability between presences and absences, and AUC $<$ 0.5 indicative of a model performing no better than random (Elith and Leathwick, 2009). Threshold-dependent metrics included the kappa statistic which ranges between -1 and $+1$, where values $<$ 0 indicate a model performing no better than random and $+1$ indicate perfect agreement with the observed values (Cohen, 1960). Although kappa scores have been shown to be affected by prevalence, i.e. the relative number of presences (Allouche et al., 2006), they were still calculated for potential insights into the effects of various resampling adjustments to RF models that affected prevalence. To provide a prevalence-controlled, threshold-dependent measure of predictive ability, the True Skill Statistic (TSS (Allouche et al., 2006);) was used. Other threshold-dependent metrics included sensitivity (portion of correctly predicted presences) and specificity (portion of correctly predicted absences). Thresholds applied to the predicted probabilities of each model were defined by the value maximising Sensitivity and Specificity which is a robust threshold method for converting continuous suitability outputs into binary maps (Liu et al., 2005) and commonly used in the marine realm (e.g., Morato et al., 2020; Beazley et al., 2021). Thresholds and threshold-dependent evaluation metrics were computed using the 'optimal.thresholds' function in the 'PresenceAbsence' R package (Freeman and Moisen, 2008).

2.3.6. Ensemble model

As several resampling options (in the case of RF models) and variable combinations (terrain-only or terrain-hydrodynamic) were explored, the decision on which version of the MaxEnt and RF models to include in the final ensemble model was collectively guided by AUC values, prediction uncertainty, overall ranking of each model's evaluation metrics, and visual inspection of their spatial predictions across the study area. Predictions from the best versions of the RF and MaxEnt models were subsequently averaged across each model's replicate outputs and weighted by each replicate's respective AUC value (n = 50/algorithm) to generate an ensemble of the two models' predictions. The degree of spatial disagreement between the models (i.e. inter-model variability) used in the ensemble model was calculated as the standard deviation between the merged rasters' values and transformed into a proportional coefficient of variation.

3. Results

3.1. Model performance

Models selected for inclusion in the ensemble model were the MaxEnt model with terrain and hydrodynamic variables, and the RF model with resampling via down-sampling and containing terrain and hydrodynamic variables. This ensemble model demonstrated the best overall performance across the range of evaluation metrics considered (Fig. 3). Area Under the Curve (AUC) of the receiver operating curve values were greatest for the ensemble (0.97 $\pm$ 0.04). All versions of RF had AUC values in between 0.89 and 0.93, whilst these were lower in MaxEnt (0.82 for both versions, Fig. 3a).

True Skill Statistic (TSS) values were high for the ensemble model (0.91 $\pm$ 0.1) and RF model with down-sampling (0.78 $\pm$ 0.06), followed by other iterations of RF terrain-hydrodynamic models with TSS values between 0.72 and 0.73 (Fig. 3b). MaxEnt had the lowest TSS values, particularly that of the MaxEnt terrain variable-only model (0.63 $\pm$ 0.21).

Models ranked similarly based on kappa, that of the ensemble being greatest (0.89 $\pm$ 0.12), followed by RF down-sampled (kappa 0.74 $\pm$ 0.06). The remaining iterations of RF terrain-hydrodynamic models had similar values for kappa, whilst that of the MaxEnt models were lower and associated with the greatest standard deviations (Fig. 3c).

Sensitivity (proportion of correctly predicted presences) was similar for MaxEnt and the ensemble models (0.96), followed by the RF down-sampled model (0.92 $\pm$ 0.06). The RF terrain variable-only model ranked lowest in terms sensitivity (0.78 $\pm$ 0.05) (Fig. 3d). Specificity (proportion of correctly predicted absences/pseudo-absences) was greatest for the ensemble (0.95 $\pm$ 0.07), followed by RF models, and lowest for MaxEnt models that had specificity values between 0.68 and 0.78 (Fig. 3e). Only in the case of the down-sampled RF model were sensitivity values greater than specificity values; all other versions of RF models performed better in terms of specificity vs sensitivity (Fig. 3d and e).

The comparatively better performance of MaxEnt models in terms of sensitivity is most likely because it predicted presences over much greater and more continuous extents (Table 2, Fig. 7), thereby increasing the likelihood that a presence point will fall somewhere within the area MaxEnt predicted as having suitable conditions. Equally, models whose binary predictions encompassed smaller areas performed better in terms of specificity. The terrain-hydrodynamic RF down-sampled and MaxEnt models performed worse than their comparators according to specificity than sensitivity, yet when they were merged to create the ensemble model, the resultant ensemble had the best specificity score, and second-best sensitivity score (Fig. 3d and e).

3.2. Role of environmental variables

3.2.1. Variable importance

In MaxEnt models, depth substantially outranked other variables in terms of permutational importance. This was most evident in the terrain variable-only MaxEnt model where depth had 94.4% permutational

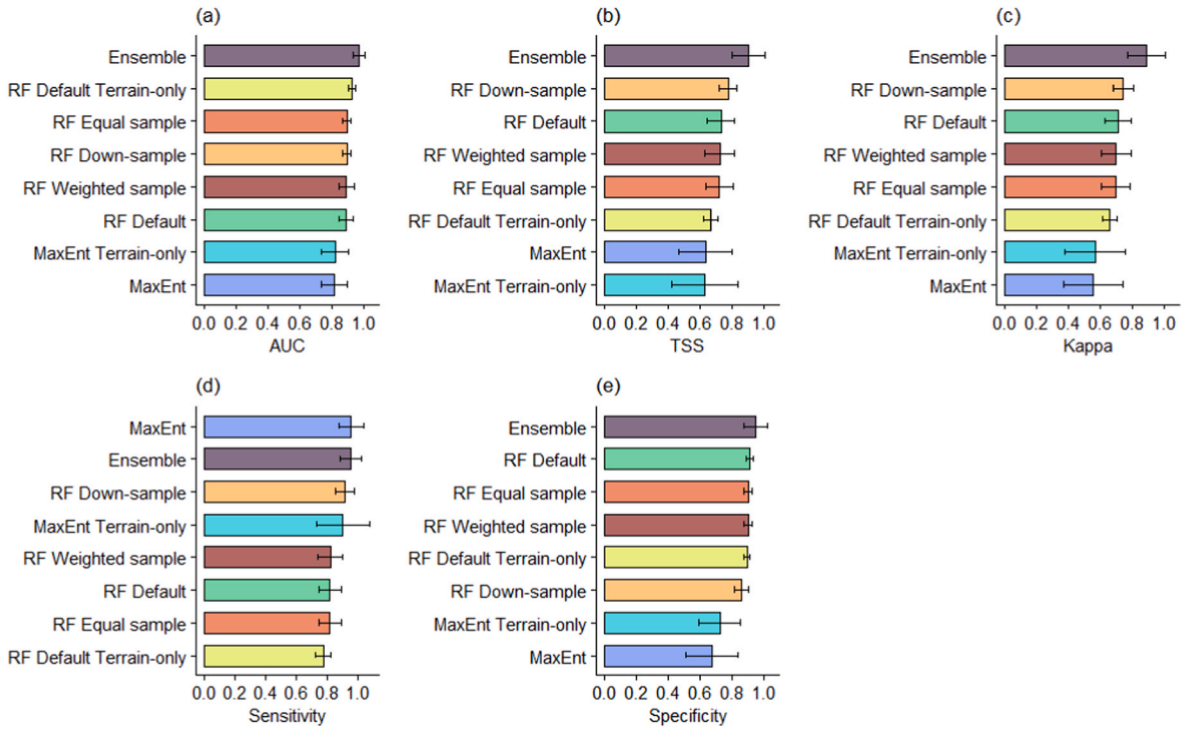

Fig. 3. Threshold-independent (A) and threshold-dependent evaluation metrics (B-E) from RF and MaxEnt models incorporating terrain-only and a combination of terrain-hydrodynamic models, using thresholds based on values maximising sensitivity and specificity Bars represent mean (±SD) of 5 x 10 cross-validated models.

Table 2
Mean thresholds (informed by values that maximise sensitivity and specificity) applied to probability predictions generated by the various models, the consequent area (km^2) likely to be most suitable for *Enallopsammia rostrata* across the study area, and its corresponding proportion of the study area.

Model	Threshold	Suitable area (km^2)	Proportion suitable area (%)
Ensemble	0.59	10 519.90	4.45
RF Weighted	0.49	10 577.57	4.47
RF Equal sample	0.62	10 652.67	4.51
RF Default	0.49	10 724.47	4.54
RF Down-sample	0.48	10 880.34	4.60
Maxent terrain-only	0.35	10 916.76	4.62
Maxent	0.24	11 571.18	4.89
RF Default, terrain-only	0.48	13 169.55	5.57

importance, and all remaining variables had less than 2.5% (Fig. 4). When incorporating hydrodynamic variables in the MaxEnt model, depth still far surpassed other variables (78.2%), although the proportional importance of other variables was greater, namely for minimum vertical velocity (11.4%) and bottom kinetic energy dissipation (4.9%).

In the terrain variable-only RF model, depth was similarly the most important variable (41.1%). However, in contrast to its MaxEnt comparator where the importance of other variables was substantially less, the RF model (run with default resampling settings) afforded greater importance to profile curvature (29.8%) and slope (21.2%) (Fig. 4). When incorporating hydrodynamic variables into the similarly set-up RF default model, the importance of depth decreased to 34.9%, followed by slope (22.8%), minimum bottom salinity (16.1%) and bottom kinetic energy dissipation (13.9%) (Fig. 4).

Most terrain-hydrodynamic RF models with resampling modifications ranked depth, slope, and bottom kinetic energy dissipation among the top three most influential variables. Specifically, in the RF down-sampled model which was identified as the top-performing version of the RF models, depth had 33.8% importance, slope 22.2%, and bottom

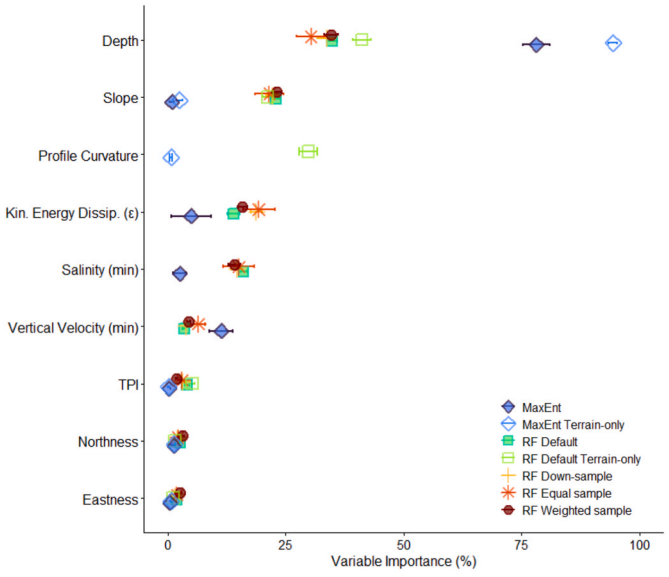

Fig. 4. Percentage importance of variables in terrain variable-only and terrain-hydrodynamic MaxEnt and RF models of *Enallopsammia rostrata*. Values are means (±SD) over 5 x 10 cross-validated models. ε = kinetic energy dissipation (log10 ε (W/kg)) of the bottom-most water layer; TPI = Topographic Position Index. Salinity and vertical velocity are minimum annual averages for the year 2009.

kinetic energy dissipation 18.8%. The importance of Topographic Position Index, eastness and northness were negligible across all models (Fig. 4).

3.2.2. *Functional responses*

The various models agreed that occurrence probability was highest between 500 and 800 m and sharply decreased as depths increased past

800 - 1000 m, after which it remained low. MaxEnt disagreed with RF at shallower depths, where the highest probabilities were predicted at around 222 m in the former, whilst in the latter it was the opposite, with probabilities showing a distinct peak between 500 and 600 m (Fig. 5a).

The influence of minimum vertical velocity (m/s) across the ranges shown was constant but sharply decreased when values neared 0, i.e. as down-welling intensity dissipated (Fig. 5b). Specifically, vertical velocities between −0.003 and −0.002 m/s, indicative of strong down-welling intensity, were associated with the greatest probabilities of occurrence in the ensemble model.

As bottom kinetic energy dissipation increased, so did the probability of *E. rostrata* occurrence. Here too did the RF and MaxEnt models demonstrate different patterns past the initial peak: a sharp increase for MaxEnt as kinetic energy dissipation increased past $-8\ \log_{10}\varepsilon$ (W/kg), but a decrease for RF past this point. The response depicted by the ensemble model instead shows a maintained elevated probability of occurrence along with elevated kinetic energy dissipation peaking at around $-8\ \log_{10}\varepsilon$ (W/kg) (Fig. 5c).

The relationship with slope was more clearly depicted by RF models, where flat slopes had near zero probability of occurrence, but this increased as slope increased and did not decrease again (Fig. 5d). This pattern was also observed in the ensemble model, where probability of occurrence increased as slopes started to get steeper around 3° after which it maintained fairly similar probabilities up to around 50° (Fig. 5d).

Topographic Position Index (TPI) values of zero (i.e. areas where the cell is at the same elevation than the average of the neighbouring cells) had a slightly negative effect on occurrence probability according to RF models, which corresponds to the similarly negative effect of flat slopes (Fig. 5e). However, in general the influence of TPI on *E. rostrata* occurrence in all models appeared to be minor. The same could be said of eastness and northness, whose ranges did not appear to have any meaningful effects on occurrence in neither RF nor MaxEnt models (Fig. 5h and i). Increasing profile curvature resulted in increased occurrence probabilities in the terrain variable-only RF and MaxEnt models (the only models where this variable was included), suggesting that increasingly convex slopes may be favourable (Fig. 5g). Occurrence peaked at salinity levels of around 34.2 PSU and 35 PSU, with a dip in probabilities between 34.5 and 34.75 PSU (Fig. 5f).

3.2.3. Extrapolation analysis

The majority of non-analogous conditions (areas of model extrapolation) were driven by differences in depth values represented in the model training data and the modelled area as a whole, comprising 72.68% of the prediction grid (Fig. S2, Table S2). Boxplots depicting environmental ranges represented in the model training data further illustrate that the majority of the prediction area is characterized by greater depth values than those in the training data (Fig. S3). Consequently, the distribution of areas with analogous conditions was the shallower sections (generally < 1800 m) on Valdivia Bank and Ewing Seamount. Importantly, the majority of presences were predicted in areas with analogous conditions (Fig. S2).

3.3. Predictions

3.3.1. Probability and uncertainty

MaxEnt models (Fig. 6a and b) had localised predictions concentrated around the shallowest locations, most likely as depth was substantially more important in these models (see section above). MaxEnt models predicted that *E. rostrata* should favour the shallowest depths in the bathymetry (Fig. 6a), which is further illustrated in the high likelihood of occurrence across seamount and knoll summits shown by the models (Fig. 6a, b, Fig. 7a and b). By contrast, the RF and ensemble models predicted greatest probabilities of occurrence below summit depths where slope was also steeper (Figs. 6 and 7).

Predictions by the RF terrain-only model appeared to be influenced

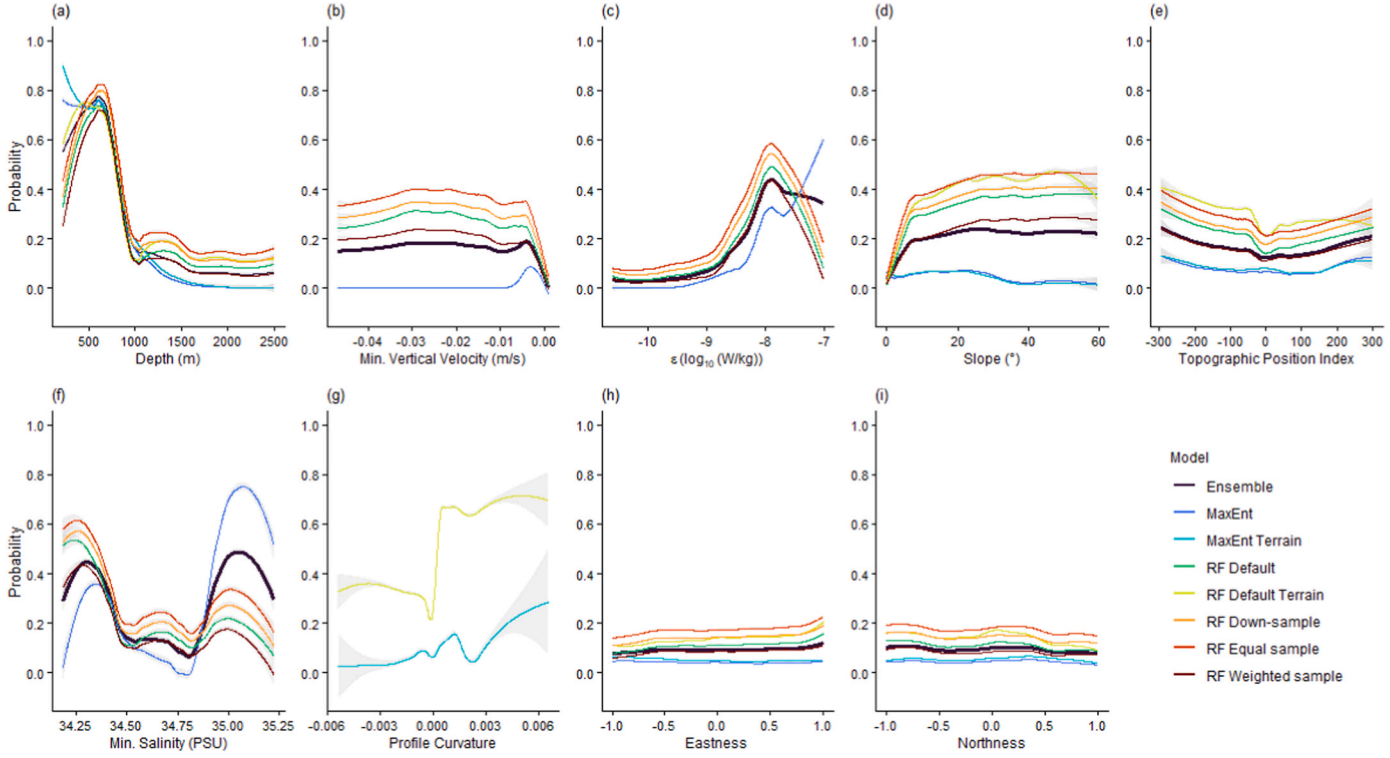

Fig. 5. Functional responses of the predicted probability of *Enallopsammia rostrata* occurrence in relation to environmental variables included in final model. Lines are polynomial regressions constructed through locally estimated scatterplot smoothing (grey shading 95% confidence interval). Note the depth range shown (A) does not depict the full depth range included in models but is shortened for illustration purposes. Note that a different set of variables were used in the terrain variable-only models and the terrain-hydrodynamic models, so not all models will appear at each variable shown here. ε = kinetic energy dissipation.

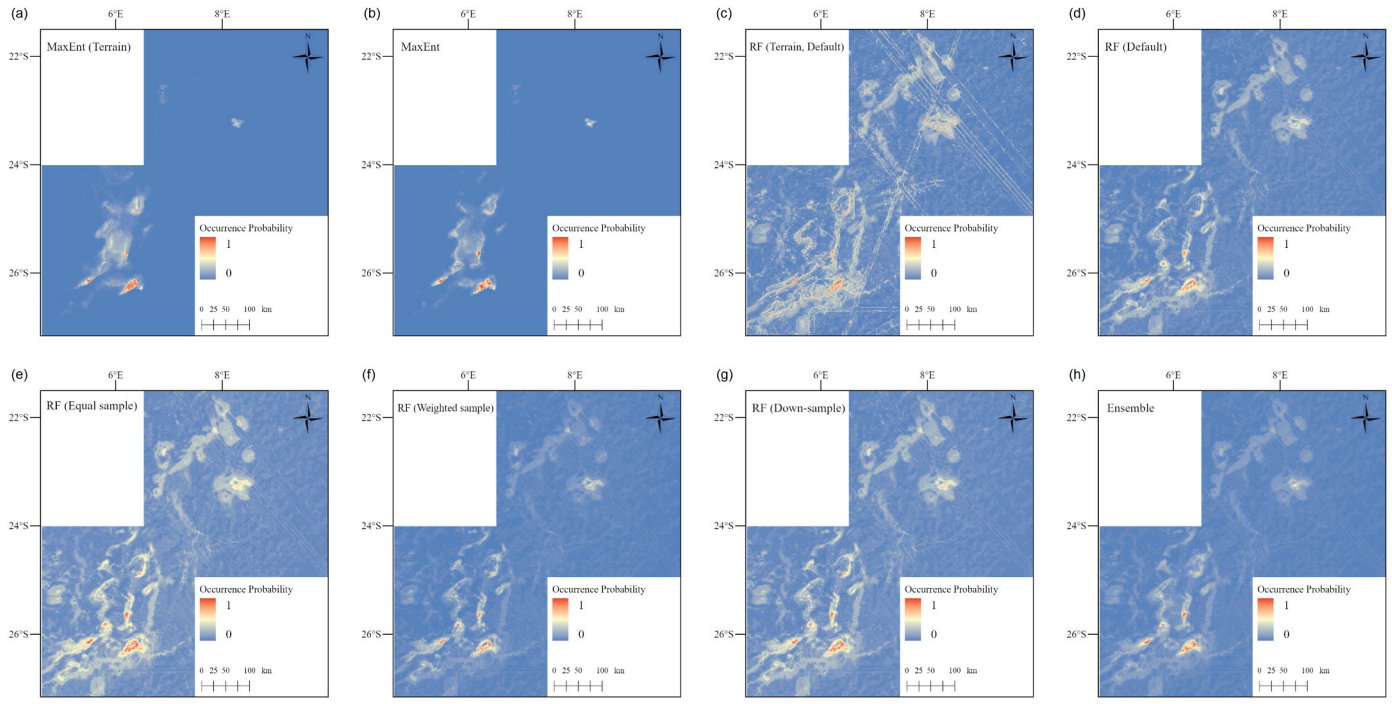

Fig. 6. Predicted occurrence of *Enallopsammia rostrata* across Valdivia Bank and Ewing Seamount, based on terrain variable-only models (A, C) and models incorporating terrain and hydrodynamic variables (B, D-G), averaged for each 5 x 10 cross-validated model. Predictions are also included for different subsampling approaches within the RF terrain-hydrodynamic models (D - G) to demonstrate effects of subsampling adjustments on model predictions. The ensemble model (H) combines predictions of the (B) MaxEnt and (G) RF down-sampled models.

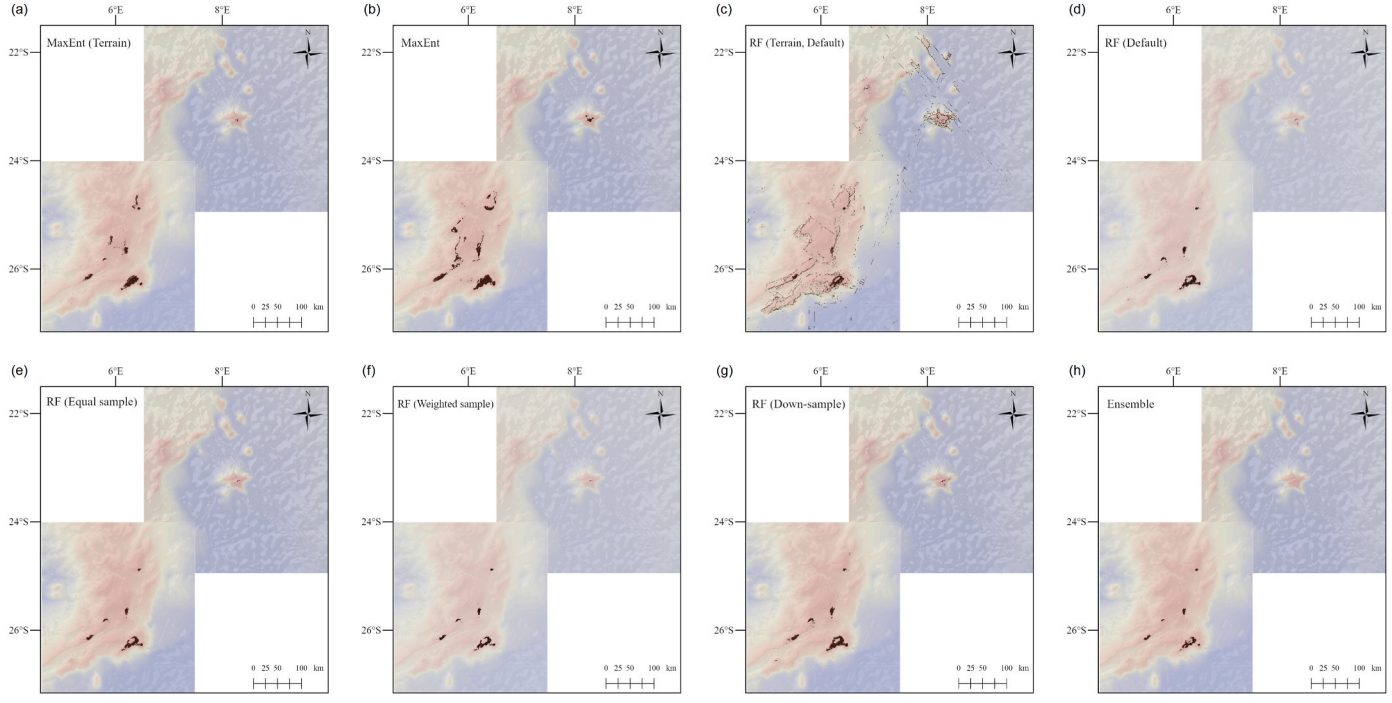

Fig. 7. Binary predictions based on model-specific thresholds (maximum sensitivity + specificity) applied to *Enallopsammia rostrata* occurrence probabilities from terrain variable-only (A, C) and terrain-hydrodynamic (B, D-H) models.

by noise-related lines in the bathymetry layer, predicting high probability of occurrence across abyssal depths where *E. rostrata* should not be found (Fig. 6c). This effect remained evident after the occurrence threshold was applied to inform binary predictions (Fig. 7c). However, inclusion of the hydrodynamic variables in the RF default model appeared to eliminate the effect of such noise on predictions (Figs. 6d and 7d). Of the various models that incorporated both terrain and hydrodynamic variables, the RF model with equal sampling generated the most widespread probability of occurrence (Fig. 6e), although this was accompanied by high uncertainty across background conditions (Fig. S4). Probability of occurrence predictions appeared similar for the RF default (Fig. 6d) and RF down-sampled (Fig. 6g) models, however the

predictions of the latter were associated with much less uncertainty than the former (Fig. S4).

Models that produced the most localised predictions included the RF model with weighted resampling (Figs. 6f and 7f) and the ensemble model (Figs. 6h and 7h). However, the RF weighted resampling model had greater and more widespread areas of uncertainty (Fig. S4f) in comparison to the ensemble model (Fig. S4h).

For all models, the lowest uncertainty coincided with areas of high likelihood of *E. rostrata* occurrence, and at topographically elevated and more complex features. Model uncertainty was most pronounced at background conditions in MaxEnt models (Fig. S4a and b), and the incorporation of hydrodynamic variables to MaxEnt models did not seem to have any meaningful effect on reducing this uncertainty. However, a comparison of prediction uncertainty between the RF terrain-only vs the RF terrain-hydrodynamic models run in default mode (Fig. S4c and Fig. S4d, respectively) showed that uncertainty across considerable areas was reduced once hydrodynamic information was accounted for. Interestingly, whilst the RF equal-sample model appeared to overpredict *E. rostrata* occurrence (Fig. 6e), and the RF weighted sample model offered more localised predictions (Fig. 6f), both models were associated with substantial uncertainty across the broader background conditions, more so than the RF default model run with no resampling modifications (Fig. S4d). The individual model with the lowest uncertainty was the RF down-sampled model (Fig. S4g), which is among the reasons why this model was selected as the best iteration of the RF models to include in the ensemble model. Indeed, when combined with the MaxEnt terrain-hydrodynamic model that had high levels of uncertainty across background conditions, the resulting ensemble model only had few places where uncertainty was high (Fig. S4h).

3.3.2. Binary predictions and suitable extent

The ensemble model applied the most conservative occurrence threshold of 0.59 for *E. rostrata* (Table 2). Application of this threshold to ensemble model prediction results in a suitable area of approximately 10 519.90 km^2, or 4.45%, of the study area (Table 2). Unsurprisingly, the likely over-predicting RF terrain-only model also suggested the greatest suitable extent, namely 13 169.55 km^2 or 5.57% of the study area.

Whilst the RF equal sample model appeared to overpredict occurrence in terms of probabilities (Fig. 6e), this model applied a higher occurrence threshold (Table 2), resulting in more localised binary predictions (Fig. 7e). MaxEnt models applied the lowest thresholds: 0.35 for the terrain variable-only model and 0.24 in the terrain-hydrodynamic model (Table 2).

Of the binary predictions generated by the ensemble model, the Valdivia Central area (Fig. 8d) had the largest portion of suitable *E. rostrata* habitat. This did not extend to the top of the summit but concentrated on areas below the summit and where slopes are also steeper (Fig. 8d). In most other areas on Valdivia Bank, suitable habitats were located at deeper knoll summits with steep slopes (Fig. 8a–c).

In most cases, predicted suitable habitat for *E. rostrata* overlapped or was near presences (Fig. 8), apart from one area at Valdivia Middle where a section of suitable habitat was predicted that was not near presence nor pseudo-absence points but is situated on a steep topographic high (Fig. 8b). The same was observed at Valdivia North (Fig. 8a) where a small, sharply elevated area in comparison to its surroundings was predicted to be suitable.

4. Discussion

This study delivers the first high-resolution spatial predictions of a VME indicator species, namely the CWC *E. rostrata*, for Valdivia Bank and Ewing seamount, located on the north-eastern ABNJ portion of the Walvis Ridge. We demonstrate that presence/background models that (i) include high-resolution hydrodynamic variables related to food supply, (ii) make model-specific adjustments compensating for class imbalance, and (iii) apply ensemble approaches that compensate for limitations of different models, can deliver reasonable predictions even when developed on a relatively small occurrence record dataset, as will be the case in many historically under-surveyed regions of the deep sea.

4.1. Model performance

Models generally agreed on those areas of highest probable occurrence of *E. rostrata,* although the MaxEnt predictions of occurrence covered greater and more continuous extents than the RF models which delivered more localised, finer resolved predictions. Area Under the Curve (AUC) values of all models were reflective of good discriminatory abilities between presences and pseudo-absences/background points (AUC > 0.7), this being greatest in the ensemble model that combined predictive outputs from the RF down-sampled and MaxEnt models, both developed on terrain and hydrodynamic variables. Whilst the AUC for the RF terrain-only model run in default mode was slightly higher than that of other versions of RF models, when viewed alongside its performance across other metrics, the nature of its predictions and accompanied uncertainty, other models performed notably better.

One of the goals of this study was to investigate the effects of adjustments to models developed on imbalanced datasets, such as in data-limited scenarios and in presence/background models. In such datasets, issues related to prevalence, i.e. the relative number of presences, can have notable effects on some threshold-dependent metrics such as the kappa statistic. When prevalence is perceived as low, kappa can be negatively affected and might not be reflective of true predictive ability (Allouche et al., 2006). Should resampling modifications be made toward a more balanced split between presence and background or pseudo-absence points, and performance then averaged over cross-validated model runs, kappa should resemble prevalence-controlled metrics like the True Skill Statistic (Allouche et al., 2006). For this reason, it is interesting to note that in terms of TSS and kappa, the RF down-sampled model outperformed other versions of RF and MaxEnt model, the latter performing the worst in this regard (Fig. 3b and c). The resampling modifications made in the RF equal sample model also balance presence and background points; however, this is done at the level of the replicate model (the 'forest') and not at the level of individual classification trees within a replicate model (Valavi et al., 2021). It therefore uses less background information, likely limiting the models' discriminatory ability between those environmental conditions that support presences vs the background. This likely explains why the RF down-sampled model performed better in this regard, as more randomised background points are used in each classification tree within a model replicate. Challenges related to prevalence in this dataset may also explain other patterns observed, such as the sharp spikes in occurrence likelihood predicted by MaxEnt models at depths < 500 m and bottom kinetic energy dissipation rates < -8 log10 ε (W/kg). As opposed to RF, many more background points were used in the MaxEnt models, and although these were selected by concentrating the background points around sampling localities, and using default MaxEnt parameters that have been shown to deal well with small presence sample sizes (Phillips and Dudík, 2008), there remains the possibility that an overall mismatch between the values of some environmental conditions are not adequately represented at the background points across the k-fold replicates used in this study. Different combinations of background points were used in each model fold, potentially adding more weight to presence point conditions for some variables (e.g. depth and kinetic energy dissipation), which may explain the sharp spikes observed (Fig. 5a–c).

Whilst the model evaluation metrics proved useful for comparing effects of model-specific adjustments, it is important to emphasize that metrics initially designed to evaluate the performance of presence/absence models may not be wholly appropriate and therefore should not be used as the only way to evaluate presence/background or presence/pseudo-absence models (Grimmett et al., 2020). A presence/background

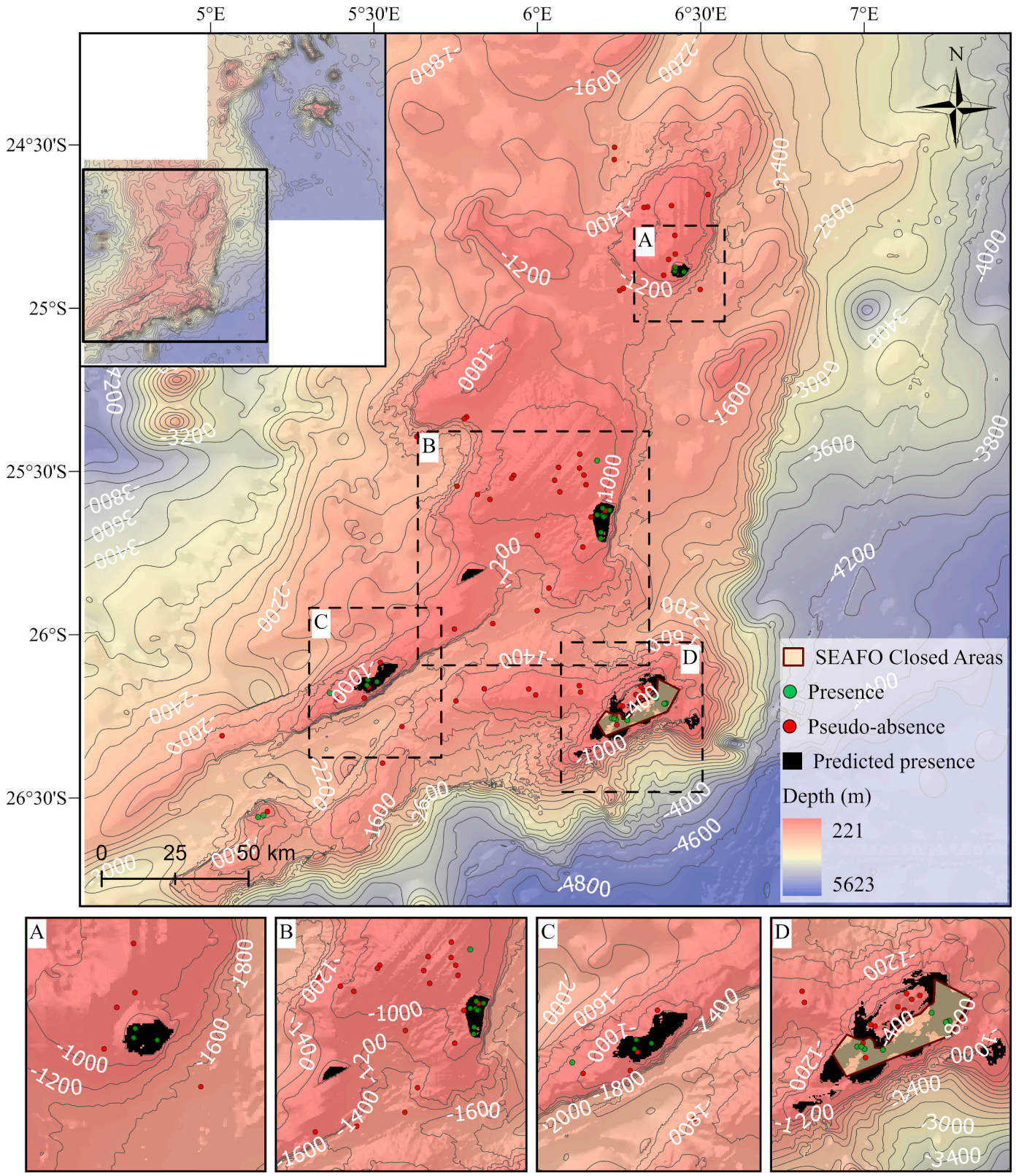

Fig. 8. Binary ensemble model predictions of *Enallopsammia rostrata* occurrence across several sections of Valdivia Bank, namely (A) Valdivia North, (B) Valdivia Middle, (C) Valdivia West and (D) Valdivia Central (names of Valdivia subareas as per Bergstad et al. (2019a). Presences are from trawl and imagery samples and pseudo-absences from trawl samples. The SEAFO closed area is presently closed to all gear types apart from bottom longlines and pots.

approach implies that while presence records are known, absences are not, and so metrics that are influenced by the model's ability to correctly predict absences (i.e. specificity) and other metrics linked therewith should be interpreted with this in mind. It is therefore also recommended that prediction uncertainty should be considered as an additional measure of model performance (Grimmett et al., 2020). Prediction uncertainty differed notably between algorithms, as well as among the different versions of RF model, which contributed to the final selection of models to include in the ensemble. Both MaxEnt models (terrain-only and terrain-hydrodynamic) exhibited pronounced uncertainty across much of the broader background (deeper) areas not covered by background points. Levels of prediction uncertainty of RF models were generally less, although there were marked differences in uncertainty levels among different versions of RF models. The down-sampled RF model had the least uncertainty (and thus greatest confidence) in its predictions, whereas uncertainty across background conditions in particular was higher in other versions of RF models. It was therefore deemed reasonable to select this model for inclusion in the ensemble.

4.2. Roles of environmental variables

The inclusion of hydrodynamic variables had several notable effects on model outputs and performance which were most pronounced in the case of the RF models. For example, the predictive maps generated by the RF terrain-only versus the RF terrain-hydrodynamic models run with default resampling settings (i.e. 'RF Default Terrain-only' and 'RF Default'), demonstrated how hydrodynamic variables substantially lowered the effects of bathymetry-induced noise on predictions. This is clearly shown when considering the nature of the predictions (Fig. 6c and d), prediction uncertainty (Fig. S4c and d), and comparisons of specificity (Fig. 3e); the lower specificity in the terrain-only model being indicative of over-prediction. The appearance of bathymetry-induced noise in RF terrain-only model predictions, and the subsequent reduction thereof in terrain-hydrodynamic versions of RF models could be due to a few factors. This includes the scale at which terrain derivatives like slope were calculated, the original resolution of hydrodynamic vs terrain variables, and the accompanied relative importance of some hydrodynamic variables. In this study, slope was calculated with a 3 x 3 cell window, a standard size often used due to its ability in capturing small-scale changes in elevation, especially in topographically complex areas (Wilson et al., 2007). This does however increase its likelihood to be affected by fine-scale noise in the bathymetry and/or properties introduced through the interpolation process when multiple elevation surfaces are merged (Albani et al., 2004). Slope was relatively important in the terrain-only RF model, which might have further accentuated noise-related effects on predictions. As the model resolution in this study was already 250 m, this trade-off is accepted, as upscaling the window size would risk the loss of meaningful information over genuinely complex areas. Moreover, the bathymetry from the more complex areas over Valdivia Bank and Ewing seamount originated from high-resolution shipboard multibeam echosounder surveys, whereas the strongest signals of noise appear in those areas supplemented with GEBCO bathymetry. The reduction in noise-related effects in the terrain-hydrodynamic RF models may be due to the original grid sizes at which hydrodynamic variables were modelled. Still considered as high resolution for hydrodynamic variables, these grids had original resolutions of 500 m and 1500 m for child and parent grids, respectively (Fig. 1b), whereas terrain grids were produced at 250 m. Interpolation to 250 m inevitably resulted in somewhat smoother grids than probably would have been achieved if hydrodynamic modelling would have been carried out at 250 m resolution, particularly at the parent grid areas that coincide with areas where bathymetry-induced noise appeared. As such, when hydrodynamic variables like kinetic energy dissipation ranked high in relative importance, this may have resulted in dampened probabilities at areas with little variation in this variable, such as over the parent grid areas. A limitation of the hydrodynamic data is that the original resolutions at which these variables were produced in Mohn et al. (2025) were limited by the computational power required to produce these variables at 250 m resolution for large areas, in combination with the fact that reliable high-resolution multibeam bathymetry is not available for the entire study area. Developing the 500 m resolution child grid resolutions over complex areas efficiently resolves small-scale variability in hydrodynamic gradients and localised flow features in these areas, whereas larger-scale gradients and kinetic energy dissipation hotspots are captured in the parent grids (Mohn et al., 2025).

The effect of hydrodynamic variables was less pronounced in MaxEnt models. These variables did not have a noticeable effect on evaluation metrics, the nature of predictions, prediction uncertainty, and were not revealed as substantially relevant in terms of permutation importance. Yet, the significance of kinetic energy dissipation in particular on model predictions persisted into the ensemble model, likely due to its importance in the RF down-sampled model (Fig. 4). This corresponds well with the suggested importance of this variable for suspension-feeding taxa in this area (Mohn et al., 2025), where it was explicitly shown that areas just below and around the summit of Valdivia Central were characterised by local maxima in kinetic energy dissipation (between -8.13 and -7.93 $\log_{10}$ ε (W/kg)), greater than across most of the study area which corresponded to high occurrence likelihood as predicted by the ensemble model (Fig. 6d–h). This effect is also strongly reflected in the functional response of *E. rostrata* occurrence to increasing kinetic energy dissipation rates (Fig. 5c). These predictions further align with Bergstad et al. (2019a) who described *E. rostrata* not to be associated with the flatter seamount and knoll summits, but rather with steeper-sloped areas below such summits and, as revealed in our study, where these slopes are met with enhanced kinetic energy dissipation.

The interplay between various hydrodynamic forces collectively influences the distribution of organic matter to CWCs. Effects of vertical velocity tend to be more pronounced at elevated and geomorphologically complex features like ridges and summit areas, promoting the transport of surface organic matter to the seafloor (Davies et al., 2009; Van Der Kaaden et al., 2021; White et al., 2008). Enhanced bottom kinetic energy dissipation, along with other processes like bottom currents and internal waves can then resuspend and redistribute the accumulated matter to CWCs, together acting to increase the rates at which they may encounter food particles (Mohn et al., 2025; Maier et al., 2023). Indeed, our results also highlight the importance of downwelling intensity, i.e. minimum vertical velocity, in models. The functional response toward this variable (Fig. 5b) indicates that strong downwelling intensity (-0.003 to -0.002 m/s) has a positive effect on *E. rostrata* occurrence. Whilst the deep sea is generally characterised as a food-limited environment, a review by Maier et al. (2023) demonstrated that where CWCs occur, delivery of organic matter to the seafloor is not always limited but may undergo temporal boosts, driven by processes like enhanced downwelling, strong currents, processes that increase turbulence, and/or vertically migrating zooplankton. Better studied CWC species like *Desmophyllum pertusum* have been shown capable of dealing well with such fluctuating resource availability, evidenced by its dietary flexibility, tissue reserves and temporally variable energy allocation and growth rates (Maier et al., 2019, 2020). Elsewhere in the Atlantic, on the Brazilian continental margin, predictive modelling of CWCs including *E. rostrata* suggested that current velocity was among the important variables driving its distribution (Barbosa et al., 2020). In this study, we excluded current velocity and instead used minimum vertical velocity and bottom kinetic energy dissipation. This was due to current velocity being strongly correlated with other variables selected, and in this case vertical velocity and kinetic energy dissipation rates were deemed more meaningful indicators of food supply processes (see Mohn et al., 2025). This does not disregard the potential value of current velocity in other studies, but it is useful to note that areas with low current velocities can still have high rates of kinetic energy conversion and dissipation, as kinetic energy dissipation can be enhanced by

processes not directly linked to current velocity, such as critical and super-critical reflection of internal tides (e.g. Van Der Kaaden et al., 2024).

In our study, depth was the most important driver, with ranges between 500 and 800 m most likely to support *E. rostrata*. It is worth nothing that the depth range predicted as optimal for *E. rostrata* in this study is narrower and shallower in comparison to its distribution across seamounts in other regions. For example, in New Zealand it has been observed up to 2147 m and has been predicted to favour 500 – 1500 m (Tracey et al., 2011), 1200 – 1700 m in Cabo Verde (Vinha et al., 2024), and 1400 – 1700 m on the New England and Corner Rise seamounts (Lapointe et al., 2020). Potential factors that may contribute to discrepancies among predictions from different regions include the variety, range and resolution of environmental variables used. The optimal depth range for *E. rostrata* on Walvis Ridge may capture other environmental conditions that promote overall suitability of the habitat, like the concentration of suspended organic material as driven by interacting terrain and hydrodynamic processes. Models developed for *E. rostrata* in New Zealand indeed excluded depth as variables such as dissolved organic carbon concentration, particulate organic matter and salinity offer greater explanatory power (Anderson et al., 2016; Tracey et al., 2011; Georgian et al., 2019). In other settings, interacting hydrodynamic processes and complex topography have been illustrated to result in the creation of a nepheloid layer (concentrated organic matter) within a certain depth band (Wilson et al., 2015). This has been suggested as a potential explanation behind areas associated with high predicted CWC occurrence, abundance and species richness in the Whittard Canyon, for example (Pearman et al., 2020). Similarly, in a study focusing on other scleractinian CWCs in the North Atlantic, aragonite saturation and depth were strongly correlated, so the former was retained as a more insightful ecological metric (Morato et al., 2020). It is therefore possible that a relationship between depth and unmeasured covariates such as nutrient concentrations may be contributing to the predictions made here, representing an avenue for future environmental sampling to quantify as such information was not available for inclusion in the present modelling dataset.

Another factor that may contribute to regional differences in forecasted suitable environmental niches may be the spatial distribution and quantity of observational data, well-known to affect model performance (Howell et al., 2022; Wisz et al., 2008). In the case of Walvis Ridge, the area is not only greatly under-sampled but previous surveys have been confined either to less-complex terrain (e.g. in the case of trawl sampling (López Abellán and Holtzhausen, 2011)) or to specific depth ranges (e. g. FAO (2016)). This also means that the ranges of other environmental variables where the species may occur may not be represented in the current dataset. For example, the functional response of *E. rostrata* to salinity showed a decrease in occurrence probability at a narrow range values, between 34.5 and 34.75 PSU (Fig. 5f). It is ecologically unlikely that *E. rostrata* will find habitats at 34.2 PSU and 35 PSU favourable, but that in between as unfavourable purely based on salinity, or that salinity alone is driving this pattern. It may well be that *E. rostrata* can be found at such salinities in the study area but is yet to be sampled there, or that other factors related to water mass characteristics correlated with salinity may be at play but have not yet been elucidated. The results of the extrapolation analysis reveal that a large area in the prediction grid is characterised by environmental conditions not observed in the training data (Table S2, Fig. S2). More survey effort is needed to address the current bias in sampling so that more presences and well as true absences across a broader range of environmental conditions can be used to improve future iterations of the model. The pseudo-absences used in RF modelling are not the same as true absences, as these are from sampling gear with unquantified catchability (i.e. trawl surveys), meaning that the target species may have been present in a grid cell but was not detected with the sampling gear. In cases where true absences are not known, like here, models developed on presence/background or presence/pseudo-absence data are likely better suited at predicting presences rather than presences and absences (Bowden et al., 2021), which may have important implications if used to support spatial planning and should be clearly communicated (Stephenson et al., 2021).

4.3. Area most likely to host Enallopsammia rostrata on walvis ridge

An area of approximately 10 519.90 km^2, translating to 4.45% of the study area across Valdivia Bank and Ewing seamount was predicted as suitable for *E. rostrata* by the ensemble model, after applying this models' occurrence threshold to the predicted probabilities. It is likely that the area currently predicted as favourable for *E. rostrata* might in fact be larger than that estimated by the current predictions, as the models presented here are underpinned by a relatively small set of occurrence records owing to limited historical sampling. Future model iterations will benefit from wider and stratified sampling, for example across varying depths, slopes, and hydrodynamic energy levels. This will provide valuable validation data that can be used to test and improve the current model. A strengthened model can also be used to generate predictions in yet unexplored areas (e.g. Bridges et al., 2023b). It will also be useful for future survey planning to include components that ensure alignment with initiatives working toward standardised sampling approaches. This will promote data interoperability and maximise the contributions that such data can deliver to advance global understanding on the distribution patterns of deep-sea biodiversity (e.g. Howell et al., 2020).

Most predicted presences for *E. rostrata* in the current study are located on Valdivia Bank, and a small portion on Ewing seamount, all of which are currently open to fishing in the SEAFO-CA, apart from a small area on Valdivia Bank that is currently closed to all gears apart from pots and bottom longlines (Fig. 8). This partial closure on Valdivia Bank is the only one that falls within the model prediction area, and contains 33.4% of the predicted presences, meaning most predicted presences (66.6%) are not captured within this closure. To date, the closures by SEAFO have been informed to some degree by a precautionary approach whereby geomorphological features expected to host VMEs were considered for inclusion in closed areas, but these closures are based coarse environmental data. Predictions from the most recent global-scale model for *E. rostrata*, developed at a 500 m resolution, indicate similar areas of a high likelihood of occurrence on Walvis Ridge (Tong et al., 2023). However, when viewed alongside the predictions generated in our study, it is clear that the coarser global-scale model likely overpredicts the extent of favourable habitat (Fig. S5). Finer resolution maps of predicted VME occurrence, like that produced for *E. rostrata* in this study, can support finer resolution spatial management planning.

Importantly, it should be noted that our study focuses on a single VME indicator species, as at the time of this publication the number of records for other indicator taxa was still insufficient for model development. Whilst *E. rostrata* is known to co-occur with some other framework-forming corals (Freiwald et al., 2004), other VME indicator species such as sponges and sea-pens have different habitat requirements, and these are yet to be mapped in this region. For example, Georgian et al. (2019) generated predictive distributions of ten VME indicator species in the South Pacific on which spatial management measures were based. The study also illustrated differences in the importance of model variables in explaining the distributions of the species included.

Work still needs to be done toward a comprehensive overview of VME habitat distribution across Walvis Ridge and the SEAFO-CA as a whole, and requires a substantial increase in the number of occurrence records, abundance information, and reliable information on true absences. As more data becomes available, future high-resolution modelling studies focusing on more VME indicator species with different environmental niches (e.g. sponges, sea-pens, and other scleractinian CWCs) can be developed and collectively be used to support spatial management plans inclusive of the various habitat types that support such taxa.

Such maps can provide useful context for ABMTs in several ways, for example through an evaluation of the effectiveness of current spatial management measures and to refine future fishery closure areas (e.g. Georgian et al., 2019), support refinement of the EBSA designation for this area, and support other spatial plans to manage and regulate multi-sector uses in ABNJ. Indeed, ABMTs are described in the recently ratified BBNJ Agreement as a method through which to manage multi-sectoral activities "with the aim of achieving particular conservation and sustainable use objectives" (United Nations, 2023). With intensifying anthropogenic impacts on ABNJ including that exerted through climate change (Franco et al., 2020), future potential deep-sea mining, and other forms of resource extraction such as oil and gas (Zhang et al., 2019), knowledge on the spatial distribution of deep-sea biodiversity and particularly VMEs will gain even more importance (McQuaid et al., 2020, 2023; Wright et al., 2021).

5. Conclusion

In conclusion, in this study we.

1) suggest that on this section of Walvis Ridge, the distribution of the VME indicator species *E. rostrata* is most strongly driven by depth, slope, and kinetic energy dissipation,
2) demonstrate that high resolution hydrodynamic variables are important explanatory variables and can strengthen SDMs, reduce uncertainty, and provide more locally resolved predictions,
3) demonstrate that steps taken to compensate for class balance in presence/background RF models, here via down-sampling, can notably improve model performance and particularly so through reducing prediction uncertainty,
4) advocate for an urgent ramping up in survey efforts in this area of the South-East Atlantic to validate and strengthen the present model, and to enable the development of predictive models for more vulnerable deep-sea species that can support present and future management and conservation efforts in this ABNJ.

CRediT authorship contribution statement

Lisa Skein: Writing – review & editing, Writing – original draft, Visualization, Methodology, Investigation, Formal analysis, Data curation, Conceptualization. **Sarah Paulus:** Writing – review & editing, Writing – original draft. **Erich Maletzky:** Writing – review & editing, Writing – original draft. **Paulus Kainge:** Writing – review & editing, Writing – original draft. **Covadonga Orejas:** Writing – review & editing, Writing – original draft, Data curation. **F. Javier Murillo:** Writing – review & editing, Writing – original draft, Methodology, Investigation. **Christian Mohn:** Writing – review & editing, Writing – original draft, Data curation. **Roberto Sarralde:** Writing – review & editing, Writing – original draft, Data curation. **Tabitha R.R. Pearman:** Writing – review & editing, Writing – original draft, Methodology, Investigation, Conceptualization. **Tobias Endjambi:** Writing – review & editing, Writing – original draft. **Veerle A.I. Huvenne:** Writing – review & editing, Writing – original draft, Supervision, Methodology, Investigation, Funding acquisition, Data curation.

D ata availability statement

- *Ensemble model predictions:* Predicted habitat suitability maps produced through the ensemble model (probability and binary predictions) can be freely accessed through the Zenodo data publisher (https://doi.org/10.5281/zenodo.21425530).
- *Occurrence records:* Benthic data from the 2008-2010 Spanish-Namibian RAPSUR surveys are available through the Ocean Biodiversity Information System (OBIS) (https://obis.org/dataset/4bdc1f6f-e16a-48b4-b995-b51bd41caa8d). Benthic data derived from the 2015 EAF-Nansen expedition: EAF-Nansen Programme-derived data are co-owned by FAO and the Programme's partner countries or RFMO/A and are subject to the Nansen Data Policy. Data requests are handled through the EAF-Nansen Programme data access portal: https://www.fao.org/in-action/eaf-nansen/data/data-access/en
- *Environmental variables:* Data from the hydrodynamic simulations in this study were performed using the ROMS-AGRIF model. This model is now frozen and has been transitioned into the CROCO (Coastal and Regional Ocean Community) project (https://www.croco-ocean.org/history/). CROCO is built upon the dynamical kernel of ROMS-AGRIF while adding new capabilities such as non-hydrostatic dynamics. At the time the Walvis Ridge simulations were developed (Mohn et al., 2025), the ROMS-AGRIF code was still publicly available. The tidal forcing data (OTIS-TPXO) and atmospheric forcing data (COADS) can be downloaded from https://www.croco-ocean.org/download/. Due to their large size and storage constraints, the 3-D hydrodynamic model output datasets are not hosted on a public repository but are available from the authors upon reasonable request. The high-resolution merged bathymetry grid for Valdivia Bank as compiled by Contreras et al. (2022) can be found on EarthRef (https://earthref.org/ERDA/2532/). Bathymetry from the 2008-2010 RAPSUR surveys can be accessed through the IEO-CSI repository (https://nodc.ieo.es/geonetwork/srv/spa/catalog.search#/metadata/urn:SDN:CDI:LOCAL:29VE200802030DTM00).

Funding sources

The research included in this manuscript received funding from the European Union's Horizon 2020 iAtlantic project (Grant Agreement No. 818123). This manuscript reflects the authors' view alone, and the European Union cannot be held responsible for any use that may be made of the information contained herein. This work was also supported by the UK Natural Environment Research Council (NERC) national capability programme CLASS ('Climate-Linked Atlantic Sector Science', NE/R015953/1) as continued in the AtlantiS programme ('Atlantic Climate and Environment Strategic Science', NE/Y005589/1).

Declaration of competing interest

The authors declare that they have no known competing financial interests or personal relationships that could have appeared to influence the work reported in this paper.

Acknowledgements

The authors thank several people that contributed to data collection and processing. This includes the scientists and crew of the RAPSUR (2008-2010) and EAF-Nansen (2015) expeditions where environmental and biological data were gathered; Tina Kutti for assistance in acquiring raw imagery that delivered a substantial contribution to the occurrence record dataset used in this study; Luis J. López-Abellán and Patricia Jiménez for providing MBES and abiotic data that underpinned terrain derivatives and hydrodynamic model variable development, respectively; and Beatriz Vinha and Michelle Taylor for assisting with taxonomic identities and queries.

This publication uses data collected through the scientific surveys with the research vessel Dr Fridtjof Nansen as part of the collaboration between the Food and Agriculture Organization of the United Nations (FAO) on behalf of the EAF-Nansen Programme and SEAFO. The EAF-Nansen Programme is a partnership between the FAO, the Norwegian Agency for Development Cooperation (Norad), and the Institute of Marine Research (IMR) in Norway for sustainable management of the fisheries in partner countries and regions.

Appendix A. Supplementary data

Supplementary data to this article can be found online at https://doi.

org/10.1016/j.dsr.2026.104758.

Data availability

Please refer to the data availability statement at the end of the manuscript. The DOI housing the mapping outputs of the study will be active following acceptance of the publication.

References

Adkins, J.F., Henderson, G.M., Wang, S.L., O'Shea, S., Mokadem, F., 2004. Growth rates of the deep-sea Scleractinia *Desmophyllum cristagalli* and *Enallopsammia rostrata*. Earth Planet Sci. Lett. 227, 481–490. https://doi.org/10.1016/J.EPSL.2004.08.022.

Albani, M., Klinkenberg, B., Andison, D.W., Kimmins, J.P., 2004. The choice of window size in approximating topographic surfaces from digital elevation models. Int. J. Geogr. Inf. Sci. 18, 577–593. https://doi.org/10.1080/13658810410001701987.

Allouche, O., Tsoar, A., Kadmon, R., 2006. Assessing the accuracy of species distribution models: prevalence, kappa and the true skill statistic (TSS). J. Appl. Ecol. 43, 1223–1232. https://doi.org/10.1111/j.1365-2664.2006.01214.x.

Althaus, F., Williams, A., Schlacher, T.A., Kloser, R.J., Green, M.A., Barker, B.A., Bax, N. J., Brodie, P., Schlacher-Hoenlinger, M.A., 2009. Impacts of bottom trawling on deep-coral ecosystems of seamounts are long-lasting. Mar. Ecol. Prog. Ser. 397, 279–294. https://doi.org/10.3354/MEPS08248.

Anderson, O.F., Guinotte, J.M., Rowden, A.A., Tracey, D.M., Mackay, K.A., Clark, M.R., 2016. Habitat suitability models for predicting the occurrence of vulnerable marine ecosystems in the seas around New Zealand. Deep-Sea Res., Part A I 115, 265–292. https://doi.org/10.1016/j.dsr.2016.07.006.

Ashford, O.S., Davies, A.J., Jones, D.O.B., 2014. Deep-sea benthic megafaunal habitat suitability modelling: a global-scale maximum entropy model for xenophyophores. Deep-Sea Res., Part A I 94, 31–44. https://doi.org/10.1016/j.dsr.2014.07.012.

Baco, A.R., Roark, E.B., Morgan, N.B., 2019. Amid fields of rubble, scars, and lost gear, signs of recovery observed on seamounts on 30- to 40-year time scales. Sci. Adv. 5, eaaw4513. https://doi.org/10.1126/sciadv.aaw4513.

Baco, A.R., Ross, R., Althaus, F., Amon, D., Bridges, A.E., Brix, S., Buhl-Mortensen, P., Colaco, A., Carreiro-Silva, M., Clark, M.R., Du Preez, C., 2023. Towards a scientific community consensus on designating vulnerable marine ecosystems from imagery. PeerJ 11, e16024. https://doi.org/10.7717/peerj.16024.

Barbet-Massin, M., Jiguet, F., Albert, C.H., Thuiller, W., 2012. Selecting pseudo-absences for species distribution models: how, where and how many? Methods Ecol. Evol. 3, 327–338. https://doi.org/10.1111/j.2041-210x.2011.00172.x.

Barbosa, R.V., Davies, A.J., Sumida, P.Y.G., 2020. Habitat suitability and environmental niche comparison of cold-water coral species along the Brazilian continental margin. Deep-Sea Res., Part A I 155, 103147. https://doi.org/10.1016/j.dsr.2019.103147.

Beazley, L., Kenchington, E., Murillo, F.J., Brickman, D., Wang, Z., Davies, A.J., Roberts, E.M., Rapp, H.-T., 2021. Climate change winner in the deep sea? Predicting the impacts of climate change on the distribution of the glass sponge *Vazella pourtalesii*. Mar. Ecol. Prog. Ser. 657, 1–23. https://doi.org/10.3354/meps.

Bell, K.L.C., Johannes, K.N., Kennedy, B.R.C., Poulton, S.E., 2025. How little we've seen: a visual coverage estimate of the deep seafloor. Sci. Adv. 11, eadp8602. https://doi.org/10.1126/sciadv.adp8602.

Bergstad, O.A., Gil, M., Høines, Å.S., Sarralde, R., Maletzky, E., Mostarda, E., Singh, L., António, M.A., Ramil, F., Clerkin, P., Campanis, G., 2019a. Megabenthos and benthopelagic fishes on southeast Atlantic seamounts. Afr. J. Mar. Sci. 41, 29–50. https://doi.org/10.2989/1814232x.2019.1571439.

Bergstad, O.A., Høines, Å.S., Sarralde, R., Campanis, G., Gil, M., Ramil, F., Maletzky, E., Mostarda, E., António, M.A., Singh, L., 2019b. Bathymetry, substrate and fishing areas of southeast Atlantic high-seas seamounts. Afr. J. Mar. Sci. 41, 11–28. https://doi.org/10.2989/1814232X.2019.1569160.

Bett, B.J., Piechaud, N., Strong, J.A., Curtis, E.J., Huvenne, V.A.I., 2025. Monitoring deep-sea cold-water coral ecosystems: 16 years of protection but no recovery on the Darwin mounds (bathyal NE Atlantic). Sci. Total Environ. 995, 180118. https://doi.org/10.1016/j.scitotenv.2025.180118.

Bouchet, P.J., Miller, D.L., Roberts, J.J., Mannocci, L., Harris, C.M., Thomas, L., 2020. Dsmextra: extrapolation assessment tools for density surface models. Methods Ecol. Evol. 11, 1464–1469. https://doi.org/10.1111/2041-210X.13469.

Bowden, D.A., Anderson, O.F., Rowden, A.A., Stephenson, F., Clark, M.R., 2021. Assessing habitat suitability models for the deep sea: is our ability to predict the distributions of seafloor fauna improving? Front. Mar. Sci. 8, 632389. https://doi.org/10.3389/fmars.2021.632389.

Breiman, L., 2001. Random forests. Mach. Learn. 45, 5–32. https://doi.org/10.1023/A:1010933404324.

Bridges, A., Howell, K., Amaro, T., Atkinson, L., Barnes, D., Bax, N., Bell, J., Bernardino, A., Beuck, L., Braga-Henriques, A., Brandt, A., Bravo, M., Brix, S., Butt, S., Carranza, A., Doti, B., Elegbede, I., Esquete, P., Freiwald, A., Gaudron, S., 2023a. Review of the central and south Atlantic shelf and deep-sea benthos: science, policy, and management. In: Sheppard, C. (Ed.), World Seas: an Environmental Evaluation, second ed. Elsevier, pp. 127–218. https://doi.org/10.1201/9781003363873-5.

Bridges, A.E.H., Barnes, D.K.A., Bell, J.B., Ross, R.E., Voges, L., Howell, K.L., 2023b. Filling the data gaps: transferring models from data-rich to data-poor deep-sea areas to support spatial management. J. Environ. Manag. 345, 118325. https://doi.org/10.1016/j.jenvman.2023.118325.

Buhl-Mortensen, L., Vanreusel, A., Gooday, A.J., Levin, L.A., Priede, I.G., Buhl-Mortensen, P., Gheerardyn, H., King, N.J., Raes, M., 2010. Biological structures as a source of habitat heterogeneity and biodiversity on the deep ocean margins. Mar. Ecol. 31, 21–50. https://doi.org/10.1111/j.1439-0485.2010.00359.x.

Clark, M.R., Althaus, F., Schlacher, T.A., Williams, A., Bowden, D.A., Rowden, A.A., 2016. The impacts of deep-sea fisheries on benthic communities: a review. ICES J. Mar. Sci. 73, i51–i69. https://doi.org/10.1093/icesjms/fsv123.

Clark, M.R., Bowden, D.A., Rowden, A.A., Stewart, R., 2019. Little evidence of benthic community resilience to bottom trawling on seamounts after 15 years. Front. Mar. Sci. 6, 63. https://doi.org/10.3389/fmars.2019.00063.

Cohen, J., 1960. A coefficient of agreement for nominal scales. Educ. Psychol. Meas. 20, 37–46. https://doi.org/10.1177/001316446002000104.

Contreras, E., García, P.J., Sager, W.W., Thoram, S., Hoernle, K., Sarralde, R., Zhou, H., 2022. Bathymetry of valdivia bank, walvis ridge, south Atlantic Ocean: implications for structure and geologic history of a hot spot plateau. G-cubed 23, e2022GC010624. https://doi.org/10.1029/2022gc010624.

Corbera, G., Iacono, C.L., Gràcia, E., Grinyó, J., Pierdominico, M., Huvenne, V.A.I., Aguilar, R., Gili, J.M., 2019. Ecological characterisation of a Mediterranean cold-water coral reef: cabliers coral mound province (Alboran Sea, western Mediterranean). Prog. Oceanogr. 175, 245–262.

Cordes, E.E., McGinley, M.P., Podowski, E.L., Becker, E.L., Lessard-Pilon, S., Viada, S.T., Fisher, C.R., 2008. Coral communities of the deep Gulf of Mexico. Deep-Sea Res., Part A I 55, 777–787. https://doi.org/10.1016/j.dsr.2008.03.005.

Costello, M.J., McCrea, M., Freiwald, A., Lundälv, T., Jonsson, L., Bett, B.J., van Weering, T.C.E., de Haas, H., Roberts, J.M., Allen, D., 2005. Role of cold-water *Lophelia pertusa* coral reefs as fish habitat in the NE Atlantic. In: Freiwald, A., Roberts, J.M. (Eds.), Cold-Water Corals and Ecosystems. Springer, Berlin, pp. 771–805. https://doi.org/10.1007/3-540-27673-4_41.

Davies, A.J., Duineveld, G.C.A., Lavaleye, M.S.S., Bergman, M.J.N., van Haren, H., 2009. Downwelling and deep-water bottom currents as food supply mechanisms to the cold-water coral *Lophelia pertusa* (Scleractinia) at the mingulay reef complex. Limnol. Oceanogr. 54, 620–629. https://doi.org/10.4319/lo.2009.54.2.0620.

Davies, A.J., Guinotte, J.M., 2011. Global habitat suitability for framework-forming cold-water corals. PLoS One 6, e18483. https://doi.org/10.1371/journal.pone.0018483.

Demopoulos, A.W.J., Bourque, J.R., Frometa, J., 2014. Biodiversity and community composition of sediment macrofauna associated with deep-sea *Lophelia pertusa* habitats in the Gulf of Mexico. Deep-Sea Res., Part A I 93, 91–103. https://doi.org/10.1016/j.dsr.2014.07.014.

Dolan, M., Grehan, A., Guinan, J., Brown, C., 2008. Modelling the local distribution of cold-water corals in relation to bathymetric variables: adding spatial context to deep-sea video data. Deep-Sea Res., Part A I 55, 1564–1579. https://doi.org/10.1016/j.dsr.2008.06.010.

Du Preez, C., Swan, K.D., Curtis, J.M.R., 2020. Cold-water corals and other vulnerable biological structures on a north Pacific seamount after half a century of fishing. Front. Mar. Sci. 7, 502446. https://doi.org/10.3389/fmars.2020.00017.

Elith, J., 2019. Machine learning, random forests and boosted regression trees. In: Brennan, L., Tri, A., Marcot, B. (Eds.), Quantitative Analyses in Wildlife Science: Wildlife Management and Conservation. Johns Hopkins University Press, pp. 281–297.

Elith, J., Leathwick, J.R., 2009. Species distribution models: ecological explanation and prediction across space and time. Annu. Rev. Ecol. Evol. Syst. 40, 677–697. https://doi.org/10.1146/annurev.ecolsys.110308.120159.

Elith, J., Phillips, S.J., Hastie, T., Dudík, M., Chee, Y.E., Yates, C.J., 2011. A statistical explanation of MaxEnt for ecologists. Divers. Distrib. 17, 43–57. https://doi.org/10.1111/j.1472-4642.2010.00725.x.

Etnoyer, P.J., Wagner, D., Fowle, H.A., Poti, M., Kinlan, B., Georgian, S.E., Cordes, E.E., 2018. Models of habitat suitability, size, and age-class structure for the deep-sea black coral *Leiopathes glaberrima* in the Gulf of Mexico. Deep-Sea Res. Part II 150, 218–228. https://doi.org/10.1016/j.dsr2.2017.10.008.

FAO, 2009. International Guidelines for the Management of Deep-Sea Fisheries in the High Seas. Rome.

FAO, 2016. Investigations of Vulnerable Marine Ecosystems (Vmes), Fisheries Resources and Biodiversity in the Convention Area of the South East Atlantic Fisheries Organisation (SEAFO), 15 January–12 February 2015. FAO–NORAD Project No: GCP/INT/003/NOR. Cruise Report Dr Fridtjof Nansen, EAF-N/2015/2. Rome.

Franco, B.C., Defeo, O., Piola, A.R., Barreiro, M., Yang, H., Ortega, L., Gianelli, I., Castello, J.P., Vera, C., Buratti, C., Pájaro, M., Pezzi, L.P., Möller, O.O., 2020. Climate change impacts on the atmospheric circulation, ocean, and fisheries in the southwest south Atlantic Ocean: a review. Clim. Change 162, 2359–2377. https://doi.org/10.1007/s10584-020-02783-6.

Freeman, E.A., Moisen, G., 2008. PresenceAbsence: an R package for presence-absence model analysis. J. Stat. Software 23 (11), 1–31. https://doi.org/10.18637/jss.v023.i11.

Freiwald, A., Fossâ, J.H., Grehan, A., Koslow, T., Roberts, J.M., 2004. Cold-Water Coral Reefs: out of sight-no Longer out of Mind. UNEP-WCMC, p. 86.

GEBCO Bathymetric Compilation Group, 2020. The GEBCO_2020 Grid - a Continuous Terrain Model of the Global Oceans and Land. British Oceanographic Data Centre, National Oceanography Centre, NERC, UK.

Georgian, S.E., Anderson, O.F., Rowden, A.A., 2019. Ensemble habitat suitability modeling of vulnerable marine ecosystem indicator taxa to inform deep-sea fisheries management in the south Pacific Ocean. Fish. Res. 211, 256–274. https://doi.org/10.1016/j.fishres.2018.11.020.

Georgian, S.E., Shedd, W., Cordes, E.E., 2014. High-resolution ecological niche modelling of the cold-water coral Lophelia pertusa in the Gulf of Mexico. Mar. Ecol. Prog. Ser. 506, 145–161. https://doi.org/10.3354/meps10816.

Gil, M., Ramil, F., 2021. Hydroids (Cnidaria, Hydrozoa) from the vema and valdivia seamounts (SE Atlantic). Eur. J. Taxon. 758, 49–96. https://doi.org/10.5852/EJT.2021.758.1425.

Glover, A.G., Wiklund, H., Chen, C., Dahlgren, T.G., 2018. Point of view: managing a sustainable deep-sea 'blue economy' requires knowledge of what actually lives there. eLife 7, e41319. https://doi.org/10.7554/elife.41319.

Grimmett, L., Whitsed, R., Horta, A., 2020. Presence-only species distribution models are sensitive to sample prevalence: evaluating models using spatial prediction stability and accuracy metrics. Ecol. Model. 431, 109194. https://doi.org/10.1016/j.ecolmodel.2020.109194.

Heiberger, R.M., Holland, B., 2004. Statistical Analysis and Data Display: an Intermediate Course with Examples in S-Plus, R and SAS. Springer, New York. https://doi.org/10.1007/978-1-4757-4284-8.

Henry, L.A., Roberts, J.M., 2007. Biodiversity and ecological composition of macrobenthos on cold-water coral mounds and adjacent off-mound habitat in the bathyal porcupine seabight, NE Atlantic. Deep-Sea Res., Part A I 54, 654–672. https://doi.org/10.1016/j.dsr.2007.01.005.

Hijmans, R., 2025. Raster: geographic data analysis and modeling. R package version 3, 6–32. https://doi.org/10.32614/CRAN.package.raster.

Hijmans, R., Brown, A., Barbosa, M., 2026. Terra: spatial data analysis. R package version 1, 9–38. https://github.com/rspatial/terra.

Hijmans, R., Phillips, S., Leathwick, J., Elith, J., 2024. Dismo: species distribution modeling. R package version 1, 3–16. https://doi.org/10.32614/CRAN.package.dismo.

Hinz, H., 2017. Impact of bottom fishing on animal forests: science, conservation, and fisheries management. In: Rossi, S., Bramanti, L., Gori, A., Orejas, C. (Eds.), Marine Animal Forests: the Ecology of Benthic Biodiversity Hotspots. Springer International Publishing, pp. 1041–1059. https://doi.org/10.1007/978-3-319-21012-4_37/figures/2.

Hitt, N.T., Sinclair, D.J., Fallon, S.J., Neil, H.L., Tracey, D.M., Komugabe-Dixson, A., Marriott, P., 2020. Growth and longevity of New Zealand black corals. Deep-Sea Res., Part A I 162, 103298. https://doi.org/10.1016/j.dsr.2020.103298.

Houlbrèque, F., McCulloch, M., Roark, B., Guilderson, T., Meibom, A., Kimball, J., Mortimer, G., Cuif, J., Dunbar, R., 2010. Uranium-series dating and growth characteristics of the deep-sea scleractinian coral: *enallopsammia rostrata* from the equatorial Pacific. Geochim. Cosmochim. Acta 74, 677–691. https://doi.org/10.1016/j.gca.2009.10.022.

Howell, K.L., Bridges, A.E., Graves, K.P., Allcock, L., la Bianca, G., Ventura-Costa, C., Donaldson, S., Downie, A.L., Furey, T., McGrath, F., Ross, R., 2022. Performance of deep-sea habitat suitability models assessed using independent data, and implications for use in area-based management. Mar. Ecol. Prog. Ser. 695, 33–51. https://doi.org/10.3354/meps14098.

Howell, K.L., Hilário, A., Allcock, A.L., Bailey, D.M., Baker, M., Clark, M.R., Colaço, A., Copley, J., Cordes, E.E., Danovaro, R., Dissanayake, A., 2020. A blueprint for an inclusive, global deep-sea ocean decade field program. Front. Mar. Sci. 7, 584861. https://doi.org/10.3389/fmars.2020.584861.

Johnson, R.A., Chawla, N.V., Hellmann, J.J., 2012. Species distribution modelling and prediction: a class imbalance problem. Proceedings - 2012 Conference on Intelligent Data Understanding (CIDU), pp. 9–16. https://doi.org/10.1109/CIDU.2012.6382186.

Jonsson, L.G., Nilsson, P.G., Floruta, F., Lundälv, T., 2004. Distributional patterns of macro- and megafauna associated with a reef of the cold-water coral *Lophelia pertusa* on the Swedish west coast. Mar. Ecol. Prog. Ser. 284, 163–171. https://doi.org/10.3354/meps284163.

Koslow, J.A., Gowlett-Holmes, K., Lowry, J.K., O'Hara, T., Poore, G.C.B., Williams, A., 2001. Seamount benthic macrofauna off southern Tasmania: community structure and impacts of trawling. Mar. Ecol. Prog. Ser. 213, 111–125. https://doi.org/10.3354/meps213111.

La Bianca, G., Rees, S., Attrill, M.J., Lombard, A.T., McQuaid, K.A., Niner, H.J., van Rein, H., Sink, K.J., Howell, K.L., 2023. A standardised ecosystem services framework for the deep sea. Front. Mar. Sci. 10, 1176230. https://doi.org/10.3389/fmars.2023.1176230/full.

Lapointe, A.E., Watling, L., France, S.C., Auster, P.J., 2020. Megabenthic assemblages in the lower bathyal (700–3000 m) on the new England and corner rise seamounts, northwest Atlantic. Deep-Sea Res., Part A I 165, 103366. https://doi.org/10.1016/j.dsr.2020.103366.

Lartaud, F., Meistertzheim, A.L., Peru, E., Le Bris, N., 2017. In situ growth experiments of reef-building cold-water corals: the good, the bad and the ugly. Deep-Sea Res., Part A I 121, 70–78. https://doi.org/10.1016/j.dsr.2017.01.004.

Lecours, V., Devillers, R., Schneider, D.C., Lucieer, V.L., Brown, C.J., Edinger, E.N., 2015. Spatial scale and geographic context in benthic habitat mapping: review and future directions. Mar. Ecol. Prog. Ser. 535, 259–284. https://doi.org/10.3354/meps11378.

Liaw, A., Wiener, M., 2002. Classification and regression by randomForest. R. News 2 (3), 18–22.

Liu, C., Berry, P.M., Dawson, T.P., Pearson, R.G., 2005. Selecting thresholds of occurrence in the prediction of species distributions. Ecography 28 (3), 385–393. https://doi.org/10.1111/j.0906-7590.2005.03957.x.

Liu, C., Newell, G., White, M., 2019. The effect of sample size on the accuracy of species distribution models: considering both presences and pseudo-absences or background sites. Ecography 42, 535–548. https://doi.org/10.1111/ecog.03188.

López Abellán, L., Holtzhausen, H., 2011. Preliminary Report of the Multidisciplinary Research Cruise on the Walvis Ridge Seamounts (Atlantic Southeast, SEAFO).

Maier, S.R., Bannister, R.J., van Oevelen, D., Kutti, T., 2020. Seasonal controls on the diet, metabolic activity, tissue reserves and growth of the cold-water coral *Lophelia pertusa*. Coral Reefs 39, 173–187. https://doi.org/10.1007/s00338-019-01886-6.

Maier, S.R., Brooke, S., De Clippele, L.H., de Froe, E., van der Kaaden, A.S., Kutti, T., Mienis, F., van Oevelen, D., 2023. On the paradox of thriving cold-water coral reefs in the food-limited deep sea. Biol. Rev. 98, 1768–1795. https://doi.org/10.1111/brv.12976.

Maier, S.R., Kutti, T., Bannister, R.J., van Breugel, P., van Rijswijk, P., van Oevelen, D., 2019. Survival under conditions of variable food availability: resource utilization and storage in the cold-water coral *Lophelia pertusa*. Limnol. Oceanogr. 64, 1651–1671. https://doi.org/10.1002/lno.11142.

McQuaid, K., Bridges, A., Howell, K., Gandra, T., de Souza, V., Currie, J., Hogg, O., Pearman, T., Bell, J., Atkinson, L., Baum, D., Bonetti, J., Carranza, A., Defeo, O., Furey, T., Gasalla, M., Golding, N., Hampton, S., Horta, S., Jones, D., Lombard, A., Manca, E., Marin, Y., Martin, S., Mortensen, P., Passadore, C., Piechaud, N., Sink, K., Yool, A., 2023. Broad-scale benthic habitat classification of the south Atlantic. Prog. Oceanogr. 214, 103042. https://doi.org/10.1016/j.pocean.2023.103042.

McQuaid, K.A., Attrill, M.J., Clark, M.R., Cobley, A., Glover, A.G., Smith, C.R., Howell, K. L., 2020. Using habitat classification to assess representativity of a protected area network in a large, data-poor area targeted for deep-sea mining. Front. Mar. Sci. 7, 558860. https://doi.org/10.3389/fmars.2020.558860.

Menegotto, A., Rangel, T.F., 2018. Mapping knowledge gaps in marine diversity reveals a latitudinal gradient of missing species richness. Nat. Commun. 9, 1–6. https://doi.org/10.1038/s41467-018-07217-7.

Mesgaran, M.B., Cousens, R.D., Webber, B.L., 2014. Here be dragons: a tool for quantifying novelty due to covariate range and correlation change when projecting species distribution models. Div. Distrib. 20 (10), 1147–1159. https://doi.org/10.1111/ddi.12209.

Mohn, C., Rengstorf, A., White, M., Duineveld, G., Mienis, F., Soetaert, K., Grehan, A., 2014. Linking benthic hydrodynamics and cold-water coral occurrences: a high-resolution model study at three cold-water coral provinces in the NE Atlantic. Prog. Oceanogr. 122, 92–104. https://doi.org/10.1016/j.pocean.2013.12.003.

Mohn, C., Schwarzkopf, F.U., García, P.J., Orejas, C., Huvenne, V.A.I., Schumacher, M., Pérez-Rodríguez, I., Sarralde Vizuete, R., López-Abellán, L.J., Dale, A.C., Devey, C., Hansen, J.L.S., Møller, E.F., Biastoch, A., 2025. Dynamics of near-bottom currents in cold-water coral and sponge areas at valdivia bank and ewing seamount, southeast Atlantic. J. Geophys. Res. Oceans 130, e2024JC021667. https://doi.org/10.1029/2024JC021667.

Montero-Serrano, J.C., Frank, N., Tisnérat-Laborde, N., Colin, C., Wu, C.C., Lin, K., Shen, C.C., Copard, K., Orejas, C., Gori, A., De Mol, L., Van Rooij, D., Reverdin, G., Douville, E., 2013. Decadal changes in the mid-depth water mass dynamics of the northeastern Atlantic margin (Bay of Biscay). Earth Planet Sci. Lett. 364, 134–144. https://doi.org/10.1016/j.epsl.2013.01.012.

Morato, T., Dominguez-Carrió, C., Mohn, C., Ocaña Vicente, O., Ramos, M., Rodrigues, L., Sampaio, Í., Taranto, G.H., Fauconnet, L., Tojeira, I., Gonçalves, E.J., Carreiro-Silva, M., 2021. Dense cold-water coral garden of *Paragorgia johnsoni* suggests the importance of the mid-atlantic ridge for deep-sea biodiversity. Ecol. Evol. 11, 16426–16433. https://doi.org/10.1002/ece3.8319.

Morato, T., González-Irusta, J.M., Dominguez-Carrió, C., Wei, C.L., Davies, A., Sweetman, A.K., Taranto, G.H., Beazley, L., García-Alegre, A., Grehan, A., Laffargue, P., Murillo, F.J., Sacau, M., Vaz, S., Kenchington, E., Arnaud-Haond, S., Callery, O., Chimienti, G., Cordes, E., Egilsdottir, H., Freiwald, A., Gasbarro, R., Gutiérrez-Zárate, C., Gianni, M., Gilkinson, K., Wareham Hayes, V.E., Hebbeln, D., Hedges, K., Henry, L.A., Johnson, D., Koen-Alonso, M., Lirette, C., Mastrototaro, F., Menot, L., Molodtsova, T., Durán Muñoz, P., Orejas, C., Pennino, M.G., Puerta, P., Ragnarsson, S., Ramiro-Sánchez, B., Rice, J., Rivera, J., Roberts, J.M., Ross, S.W., Rueda, J.L., Sampaio, Í., Snelgrove, P., Stirling, D., Treble, M.A., Urra, J., Vad, J., van Oevelen, D., Watling, L., Walkusz, W., Wienberg, C., Woillez, M., Levin, L.A., Carreiro-Silva, M., 2020. Climate-induced changes in the suitable habitat of cold-water corals and commercially important deep-sea fishes in the north Atlantic. Glob. Chang. Biol. 26, 2181–2202. https://doi.org/10.1111/gcb.14996.

Mortensen, P.B., Buhl-Mortensen, L., Gebruk, A.V., Krylova, E.M., 2008. Occurrence of deep-water corals on the mid-atlantic ridge based on MAR-ECO data. Deep sea Res. Part II: Topical Stud. Oceanogr 55, 142–152. https://doi.org/10.1016/j.dsr2.2007.09.018.

Muñoz, P., Sayago-Gil, M., Murillo, F., Del Río, J., López-Abellán, L., Sacau, M., Sarralde, R., 2012. Actions taken by fishing nations towards identification and protection of vulnerable marine ecosystems in the high seas: the Spanish case (atlantic ocean). Mar. Policy 36, 536–543. https://doi.org/10.1016/j.marpol.2011.09.005.

Pearman, T., Robert, K., Callaway, A., Hall, R., Iacono, C., Huvenne, V.A.I., 2020. Improving the predictive capability of benthic species distribution models by incorporating oceanographic data—Towards holistic ecological modelling of a submarine canyon. Prog. Oceanogr. 184, 102338. https://doi.org/10.1016/j.pocean.2020.102338.

Pérez-Díaz, L., Eagles, G., 2017. South Atlantic paleobathymetry since early Cretaceous. Sci. Rep. 7, 1–16. https://doi.org/10.1038/s41598-017-11959-7.

Phillips, S.B., Aneja, V.P., Kang, D., Arya, S.P., 2006. Maximum entropy modeling of species geographic distributions. Ecol. Model. 190, 231–259. https://doi.org/10.1016/j.ecolmodel.2005.03.026.

Phillips, S.J., Anderson, R.P., Dudík, M., Schapire, R.E., Blair, M.E., 2017. Opening the black box: an open-source release of maxent. Ecography 40 (7), 887–893. https://doi.org/10.1111/ecog.03049.

Phillips, S.J., Dudík, M., 2008. Modeling of species distributions with maxent: new extensions and a comprehensive evaluation. Ecography 31, 161–175. https://doi.org/10.1111/j.0906-7590.2008.5203.x.

Posit team, 2026. Rstudio: Integrated Development Environment for R. Posit Software. PBC, Boston, MA. URL. http://www.posit.co/.

Pourtalès, L.F., 1878. Corals. In: reports on the dredging operations of the U.S. Coast survey steamer "Blake". Bulletin of the Museum of Comparative Zoology at Harvard College, in Cambridge 5, 197–212 pl. 1.

Price, D.M., Robert, K., Callaway, A., Lo Iacono, C., Hall, R.A., Huvenne, V.A.I., 2019. Using 3D photogrammetry from ROV video to quantify cold-water coral reef structural complexity and investigate its influence on biodiversity and community assemblage. Coral Reefs 38, 1007–1021. https://doi.org/10.1007/s00338-019-01827-3.

Puerta, P., Johnson, C., Carreiro-Silva, M., Henry, L.A., Kenchington, E., Morato, T., Kazanidis, G., Rueda, J.L., Urra, J., Ross, S., Wei, C.L., González-Irusta, J.M., Arnaud-Haond, S., Orejas, C., 2020. Influence of water masses on the biodiversity and biogeography of deep-sea benthic ecosystems in the north Atlantic. Front. Mar. Sci. 7, 511374. https://doi.org/10.3389/fmars.2020.00239.

Rengstorf, A., Mohn, C., Brown, C., Wisz, M., Grehan, A., 2014. Predicting the distribution of deep-sea vulnerable marine ecosystems using high-resolution data: considerations and novel approaches. Deep-Sea Res. Part I Oceanogr. Res. Pap. 93, 72–82. https://doi.org/10.1016/j.dsr.2014.07.007.

Rengstorf, A.M., Yesson, C., Brown, C., Grehan, A.J., 2013. High-resolution habitat suitability modelling can improve conservation of vulnerable marine ecosystems in the deep sea. J. Biogeogr. 40, 1702–1714. https://doi.org/10.1111/jbi.12123.

Robert, K., Jones, D.O.B., Roberts, J.M., Huvenne, V.A.I., 2016. Improving predictive mapping of deep-water habitats: considering multiple model outputs and ensemble techniques. Deep-Sea Res. Part I Oceanogr. Res. Pap. 113, 80–89. https://doi.org/10.1016/j.dsr.2016.04.008.

Robinson, O.J., Ruiz-Gutierrez, V., Fink, D., 2018. Correcting for bias in distribution modelling for rare species using citizen science data. Divers. Distrib. 24, 460–472. https://doi.org/10.1111/ddi.12698.

Rogers, A.D., Baco, A., Griffiths, H., Hart, T., Hall-Spencer, J.M., 2007. Corals on seamounts. In: Pitcher, T.J., Morato, T., Hart, P.J.B., Clark, M.R., Haggen, N., Santos, R. (Eds.), Seamounts: Ecology, Fisheries and Conservation. Blackwell Publishing, Blackwell, Oxford, pp. 141–169.

Rowden, A.A., Anderson, O.F., Georgian, S.E., Bowden, D.A., Clark, M.R., Pallentin, A., Miller, A., 2017. High-resolution habitat suitability models for the conservation and management of vulnerable marine ecosystems on the Louisville seamount Chain, South Pacific Ocean. Front. Mar. Sci. 4, 335. https://doi.org/10.3389/fmars.2017.00335.

Secretariat of the Convention on Biological Diversity, 2020. Ecologically or Biologically Significant Marine Areas (Ebsas). Special Places in the World's Oceans. Volume 6: South-Eastern Atlantic Ocean. Secretariat of the Convention on Biological Diversity, Montreal, p. 108.

Shantharam, A., Poti, M., Winship, A., Lau, Y., Coleman, H., Weissman, D., Eaton, R., McGuinn, R., Cebrian, J., Hourigan, T., 2025. Multi-taxon predictions of deep-sea corals and sponges from stacked species distribution models in the United States West Coast exclusive economic zone and relation to trawl closure zones. Divers. Distrib. 31, e70005. https://doi.org/10.1111/ddi.70005.

Stephenson, F., Rowden, A.A., Anderson, O.F., Pitcher, C.R., Pinkerton, M.H., Petersen, G., Bowden, D.A., 2021. Presence-only habitat suitability models for vulnerable marine ecosystem indicator taxa in the south Pacific have reached their predictive limit. ICES J. Mar. Sci. 78 (8), 2830–2843. https://doi.org/10.1093/icesjms/fsab162.

Stevenson, A., Mitchell, F.J.G., Davies, J.S., 2015. Predation has no competition: factors influencing space and resource use by echinoids in deep-sea coral habitats, as evidenced by continuous video transects. Mar. Ecol. 36, 1454–1467. https://doi.org/10.1111/maec.12245.

Strömberg, S.M., Larsson, A.I., 2025. Field trials testing material composition and surface complexity and the effects on benthic faunal recruitment at a cold-water coral reef site. Front. Environ. Sci. 13, 1561412. https://doi.org/10.3389/fenvs.2025.1561412.

Thuiller, W., Georges, D., Engler, R., Breiner, F., Georges, M., 2016. biomod2: ensemble platform for species distribution modelling. R Package version 3 (3), r539.

Tong, R., Davies, A.J., Yesson, C., Yu, J., Luo, Y., Zhang, L., Burgos, J.M., 2023. Environmental drivers and the distribution of cold-water corals in the global ocean. Front. Mar. Sci. 10, 1217851. https://doi.org/10.3389/fmars.2023.1217851.

Tracey, D.M., Rowden, A.A., Mackay, K.A., Compton, T., 2011. Habitat-forming cold-water corals show affinity for seamounts in the New Zealand region. Mar. Ecol. Prog. Ser. 430, 1–22. https://doi.org/10.3354/meps09164.

UNGA, 2006. United Nations General Assembly Resolution 61/105. Sustainable Fisheries, Including Through the 1995 Agreement for the Implementation of the Provisions of the United Nations Convention on the Law of the Sea of 10 December 1982 Relating to the Conservation and Management of Straddling Fish Stocks and Highly Migratory Fish Stocks, and Related Instruments.

United Nations, 2023. Agreement Under the United Nations Convention on the Law of the Sea on the Conservation and Sustainable Use of Marine Biological Diversity of Areas Beyond National Jurisdiction. Adopted 19 June 2023, UN Doc A/CONF.232/2023/4.

Urbanek, S., 2026. rJava: low-level R to Java interface. R package version 1.0-18. https://doi.org/10.32614/CRAN.package.rJava.

Valavi, R., Elith, J., Lahoz-Monfort, J.J., Guillera-Arroita, G., 2021. Modelling species presence-only data with random forests. Ecography 44, 1731–1742. https://doi.org/10.1111/ecog.05615.

Valavi, R., Guillera-Arroita, G., Lahoz-Monfort, J.J., Elith, J., 2022. Predictive performance of presence-only species distribution models: a benchmark study with reproducible code. Ecol. Monogr. 92, e01486. https://doi.org/10.1002/ecm.1486.

Van Der Kaaden, A.S., Mohn, C., Gerkema, T., Maier, S.R., de Froe, E., van de Koppel, J., Rietkerk, M., Soetaert, K., van Oevelen, D., 2021. Feedbacks between hydrodynamics and cold-water coral mound development. Deep-Sea Res., Part A I 178, 103641. https://doi.org/10.1016/j.dsr.2021.103641.

Van Der Kaaden, A.S., Van Oevelen, D., Mohn, C., Soetaert, K., Rietkerk, M., Van De Koppel, J., Gerkema, T., 2024. Resemblance of the global depth distribution of internal-tide generation and cold-water coral occurrences. Ocean Sci. 20, 569–587. https://doi.org/10.5194/os-20-569-2024.

Van Oevelen, D., Duineveld, G., Lavaleye, M., Mienis, F., Soetaert, K., Heip, C.H.R., 2009. The cold-water coral community as hotspot of carbon cycling on continental margins: a food-web analysis from rockall bank (northeast Atlantic). Limnol. Oceanogr. 54, 1829–1844. https://doi.org/10.4319/lo.2009.54.6.1829.

Venables, W.N., Ripley, B.D., 2002. Modern Applied Statistics with S, fourth ed. Springer, New York. ISBN 0-387-95457-0.

Vignali, S., Barras, A.G., Arlettaz, R., Braunisch, V., 2020. SDMtune: an R package to tune and evaluate species distribution models. Ecol. Evol. 10 (20), 11488–11506. https://doi.org/10.1002/ece3.6786.

Vinha, B., Murillo, F.J., Schumacher, M., Hansteen, T.H., Schwarzkopf, F.U., Biastoch, A., Kenchington, E., Piraino, S., Orejas, C., Huvenne, V.A.I., 2024. Ensemble modelling to predict the distribution of vulnerable marine ecosystems indicator taxa on data-limited seamounts of Cabo Verde (NW Africa). Diversity Distrib 30. https://doi.org/10.1111/ddi.13896.

White, M., Bashmachnikov, I., Arístegui, J., Martins, A., 2008. Physical processes and seamount productivity. In: Seamounts: Ecology, Fisheries & Conservation, pp. 62–84. https://doi.org/10.1002/9780470691953.ch4.

Wilson, A.M., Raine, R., Mohn, C., White, M., 2015. Nepheloid layer distribution in the whittard canyon, NE Atlantic margin. Mar. Geol. 367, 130–142. https://doi.org/10.1016/j.margeo.2015.06.002.

Wilson, M.F.J., O'Connell, B., Brown, C., Guinan, J.C., Grehan, A.J., 2007. Multiscale terrain analysis of multibeam bathymetry data for habitat mapping on the continental slope. Mar. Geodesy 30, 3–35. https://doi.org/10.1080/01490410701295962.

Wiltshire, K.H., Tanner, J.E., Althaus, F., Sorokin, S.J., Williams, A., 2018. Predicting environmental suitability for key benthic species in an ecologically and economically important deep-sea environment. Deep Sea Res. Part II 157–158, 121–133. https://doi.org/10.1016/j.dsr2.2018.06.011.

Winship, A.J., Thorson, J.T., Clarke, M.E., Coleman, H.M., Costa, B., Georgian, S.E., Gillett, D., Grüss, A., Henderson, M.J., Hourigan, T.F., Huff, D.D., 2020. Good practices for species distribution modeling of deep-sea corals and sponges for resource management: data collection, analysis, validation, and communication. Front. Mar. Sci. 7, 303. https://doi.org/10.3389/fmars.2020.00303.

Wisz, M.S., Hijmans, R.J., Li, J., Peterson, A.T., Graham, C.H., Guisan, A., Elith, J., Dudík, M., Ferrier, S., Huettmann, F., Leathwick, J.R., Lehmann, A., Lohmann, L., Loiselle, B.A., Manion, G., Moritz, C., Nakamura, M., Nakazawa, Y., Overton, J.M.C., Phillips, S.J., Richardson, K.S., Scachetti-Pereira, R., Schapire, R.E., Soberón, J., Williams, S.E., Zimmermann, N.E., 2008. Effects of sample size on the performance of species distribution models. Divers. Distrib. 14, 763–773. https://doi.org/10.1111/j.1472-4642.2008.00482.x.

Wright, G., Gjerde, K.M., Johnson, D.E., Finkelstein, A., Ferreira, M.A., Dunn, D.C., Chaves, M.R., Grehan, A., 2021. Marine spatial planning in areas beyond national Jurisdiction. Mar. Policy 132, 103384. https://doi.org/10.1016/j.marpol.2018.12.003.

Yánez-Suárez, A., Van Audenhaege, L., Eddy, T., Robert, K., 2024. Fine-scale variability in habitat selection and niche differentiation between sponges and cold-water corals on vertical walls of the Charlie-Gibbs Fracture zone. Deep Sea Res. Part II, 105437. https://doi.org/10.1016/j.dsr2.2024.105437.

Yesson, C., Bedford, F., Rogers, A.D., Taylor, M.L., 2017. The global distribution of deep-water Antipatharia habitat. Deep Sea Res. Part II 145, 79–86. https://doi.org/10.1016/j.dsr2.2015.12.004.

Zhang, G., Qu, H., Chen, G., Zhao, C., Zhang, F., Yang, H., Zhao, Z., Ma, M., 2019. Giant discoveries of oil and gas fields in global deepwaters in the past 40 years and the prospect of exploration. J. Nat. Gas Geosci. 4, 1–28. https://doi.org/10.1016/j.jngss.2019.03.002.

Zhao, Z., Xiao, N., Shen, M., Li, J., 2022. Comparison between optimized MaxEnt and random forest modeling in predicting potential distribution: a case study with *Quasipaa boulengeri* in China. Sci. Total Environ. 842, 156867. https://doi.org/10.1016/j.scitotenv.2022.156867.

Zibrowius, H., Gili, J.M., 1990. Deep-water Scleractinia (Cnidaria: anthozoa) from Namibia, South Africa, and Walvis ridge, southeastern Atlantic. Sci. Mar. 54, 19–46.

Zuur, A.F., Ieno, E.N., Walker, N., Saveliev, A.A., Smith, G.M., 2009. Mixed Effects Models and Extensions in Ecology with R. Springer, New York, NY. https://doi.org/10.1007/978-0-387-87458-6.